ARMY RESEARCH LABORATORY

An Adaptation of Walker-Anderson Model Elements Into the Frank-Zook Penetration Model for Use in MUVES

by Steven B. Segletes

ARL-TR-2336

September 2000

20001208 066

Army Research Laboratory

Aberdeen Proving Ground, MD 21005-5066

ARL-TR-2336   **September 2000**

An Adaptation of Walker-Anderson Model Elements Into the Frank-Zook Penetration Model for Use in MUVES

Steven B. Segletes
Weapons and Materials Research Directorate, ARL

Abstract

The performance of the well-respected Frank-Zook (FZ) penetration algorithm is examined in light of an anticipated class of target technology involving laminated targets whose layers are thin relative to the projectile diameter (in the limiting case, this target class incorporates functionally graded materials). Because of the manner in which the FZ algorithm anticipates changes in material properties along the shotline of the penetrator, the algorithm is susceptible to inaccuracy precisely when the target layers along the shotline are thin relative to the projectile diameter. Though the problem can be quite severe when the target-layer thickness is a fraction of the projectile diameter, the effect is still evident to a much lesser extent, even as the target-element thickness is increased to several projectile diameters. A remedy to this type of problem is offered, accomplished by way of novel adaptation of elements of a model by Walker and Anderson into the FZ framework. In doing so, the target's material- and nonsteady-kinematic properties are dynamically composed via an integration through the plastic zone in the target, ahead of the rod/target interface. Additionally, a model to predict the crater-diameter profile resulting from a modeled penetration event is optionally offered as a calculation enhancement. The modeling remedies and enhancements proposed herein are offered for incorporation into the U.S. Army Research Laboratory's (ARL) modular Unix-based vulnerability estimation suite (MUVES) code, to be part of ARL's vulnerability/lethality (V/L) calculation methodology.

Table of Contents

INTENTIONALLY LEFT BLANK.

List of Figures

INTENTIONALLY LEFT BLANK.

1. Introduction

Modifications have been made to the Frank-Zook (FZ) penetration algorithm, for inclusion into the modular Unix-based vulnerability estimation suite (MUVES) code [1] of the U. S. Army Research Laboratory's (ARL) Survivability/Lethality Analysis Directorate (SLAD). The FZ algorithm is composed of extensions to the Tate-Alekseevskii (TA) [2, 3] one-dimensional (1–D) model of penetration mechanics, is described in section 9.3 of BRL-MR-3960 [4], and is currently a part of SLAD's terminal-ballistic, vulnerability/lethality (V/L) methodology. The current modifications to FZ methodology have been made under the auspices of the Target Interaction Lethality/Vulnerability (TILV) Workpackage, a joint program between ARL's SLAD and Weapons and Materials Research Directorate (WMRD).

2. Motivation

One of the many enhancements possessed by FZ methodology over the TA equations is the ability of the eroding penetrator to sense a change in target properties (*i.e.*, a target/target interface) in advance of the penetrator actually reaching that property interface. This adaptation reflects the long-understood principle that a target's resistance to penetration is composed of an integration of properties in a finite volume of target material ahead of the actual penetrator/target interface (*e.g.*, Wright and Frank [5]). When this finite volume of target material, contributing to the target resistance, crosses the boundary of a property interface, the target properties on both sides of the interface will contribute to the net resistance.

The FZ penetration algorithm can, therefore, accurately sense and respond to the situation where, for example, the penetration channel proceeds from a weak target element into a strong target element. The effective resistance offered by the target would gradually and smoothly transition from the weak value, just reaching the strong value of resistance as the penetrator/target interface reaches the strong target element. If a rod of diameter D is penetrating target element i, the influence of target element $i+1$ upon the effective target resistance $\overline{H}$ is computed by the FZ model as

$$\overline{H} = H_i + \left(H_{i+1} - H_i\right)e^{-2T_{res}/3D} \; , \tag{1}$$

1

where $H_{(\ )}$ are the target-element component resistances and T_{res} is the residual, normal thickness of target element i yet to be penetrated. In the absence of this modeling enhancement, the transition in target resistance would be unrealistically abrupt.

However, implementing this realistic enhancement within the FZ algorithm is accomplished only a single interface at a time (*i.e.*, target elements $i+2$, *etc.* do not affect the effective resistance). Thus, if the finite target volume contributing to the target resistance were to realistically entrain several target/target interfaces, the FZ algorithm would account only for the one closest to the penetrator/target interface. Such a situation can realistically arise in several situations. One is where there exists a target composed of elements that are thin compared to the penetrator diameter, possibly as in the case of targets designed for small- and medium-caliber threats. Another situation in which several target/target interfaces could be entrained in the zone of target material contributing to target resistance would be the situation where a target element is barely clipped by the penetrator shotline. This latter situation can arise even if the individual target elements are otherwise thick. And since, from the point of view of MUVES calculation, the process of selecting and calculating penetrator shotline geometries is fully automated, the user of MUVES has little or no control in preventing very thin target elements from arising along a given shotline geometry, even for large-caliber targets.

Two examples are provided here to demonstrate the nature by which thin target elements can inhibit the ability of the FZ algorithm to properly account for interface transition. In the first example, a length-to-diameter (L/D) 3 tungsten alloy penetrator of 48 mm length strikes a 50 mm plate (a super strong aluminum). In the baseline case, the 50 mm target is composed of a single plate, whereas, in the test case, it is composed of a 48 mm plate followed by a 2 mm plate of identical properties. Ballistically, these two cases should respond in a similar fashion. The properties and geometry of the simulation are given in Table 1. The results, however, depicted in Figures 1–2, show otherwise. The normalized penetration vs. striking velocity plot (Figure 1) shows discrepancies approaching 100% in penetration at velocities in the 900 m/s range.

The reason for this discrepancy can be seen by examining the target resistance vs. position plot (Figure 2). In the more realistically portrayed 50 mm single-element target, the nominal

Table 1. Material and Geometry Parameters for Example 1

PENETRATOR

L_0 (mm)	D (mm)	L/D	ρ_P (g/cm^3)	Y_0 (GPa)	k_P
48	16	3	17.3	1.9	0.5

TARGET No.1: SINGLE PLATE, 50 mm (BASELINE)

Plate No.	Thickness (mm)	ρ_T (g/cm^3)	H (GPa)	H_{SPALL} (GPa)	k_T
1	50	2.7	5	1	0.5

TARGET No. 2: 48 mm PLATE + 2 mm PLATE (TEST CASE)

Plate No.	Thickness (mm)	ρ_T (g/cm^3)	H (GPa)	H_{SPALL} (GPa)	k_T
1	48	2.7	5	N/A	0.5
2	2	2.7	5	1	0.5
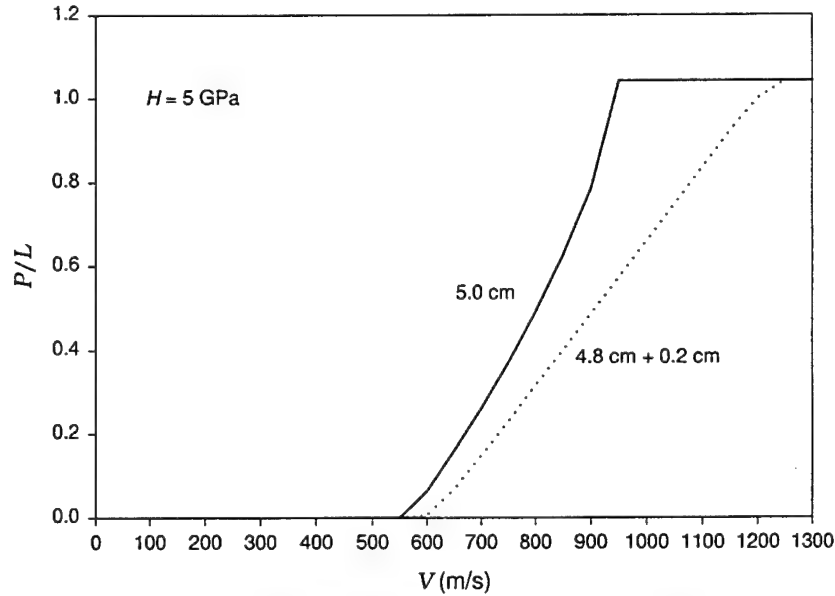
Figure 1. Effect of thin backing plate on FZ model.

target resistance of 5 GPa is seen to immediately, but gradually, decay through the thickness of the target, eventually reaching the free-surface (spall) limit strength (for this example, designated as 1 GPa). This monotonic decay in target resistance is brought on by the fact that the free surface at the rear of the target is increasingly unable to provide the support necessary to keep the target resistance at its nominal value. By contrast, the 48 + 2 mm target retains its nominal resistance out to 48 mm of target depth before the FZ algorithm even becomes aware that a free surface exists, 2 mm hence, to degrade target resistance. In essence, the 48 mm target element never detected the
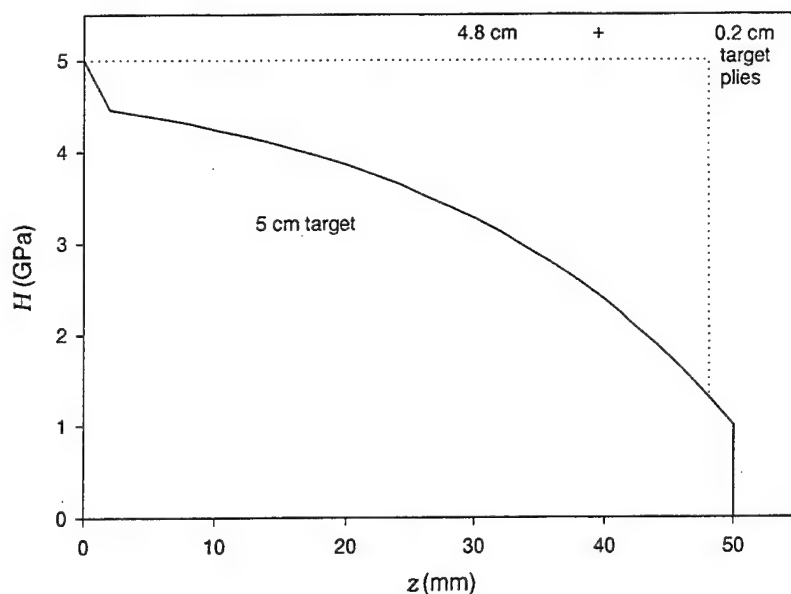
Figure 2. Comparison of Resistance vs. Location for 50 mm target and 48 + 2 mm target.

rear surface of the target, but only the subsequent 2 mm ply with identical properties to its own. It was up to the 2 mm ply to detect the target rear surface. But by then, the error had already been introduced, resulting in a vastly overestimated penetration resistance of the target. The discrepancy in predicted target penetrations is thus explained.

In the second example, whose description is provided in Table 2, the baseline target is nominally composed of two 25 mm layers, followed by an air gap and a residual rolled homogeneous armor (RHA) target. While both 25 mm layers have the density of aluminum, the first has a 3 GPa target resistance, while the second has a much stronger 8 GPa resistance. In the test case of this problem, a weak 0.1 GPa film of 0.1 mm thickness is inserted between the two 25 mm plies. Clearly, such a minute modification to the target recipe should have no net effect.

Yet, the normalized penetration vs. striking velocity plot (Figure 3) shows a vast discrepancy (often a factor of 2) between the baseline and test cases. As in the prior example, the source of the problem is identical. In the baseline case, without the interply film, penetration through the first ply becomes progressively more difficult as the 8 GPa strong target element is detected and approached. In the test case, by comparison, the 8 GPa ply is never detected while penetrating the first ply. Rather, only the weak 0.1 GPa ply is detected, and so penetration through the first ply becomes progressively easier as the rear of the first ply is approached. The target resistance vs. position plot

4

Table 2. Material and Geometry Parameters for Example 2

PENETRATOR

L_0 (mm)	D (mm)	L/D	ρ_P (g/cm^3)	Y_0 (GPa)	k_P
48	16	3	17.3	1.9	0.5

TARGET No.1: NO WEAK INTERPLY (BASELINE)

Plate No.	Thickness (mm)	ρ_T (g/cm^3)	H (GPa)	H_{SPALL} (GPa)	k_T
1	25	2.7	3	N/A	0.5
2	25	2.7	8	2	0.5
3 (air)	80	~0	0	N/A	0.5
4	∞	7.85	5	N/A	0.5

TARGET No. 2: THIN (0.1 mm) WEAK (0.1 GPa) INTERPLY FILM LAYER (TEST CASE)

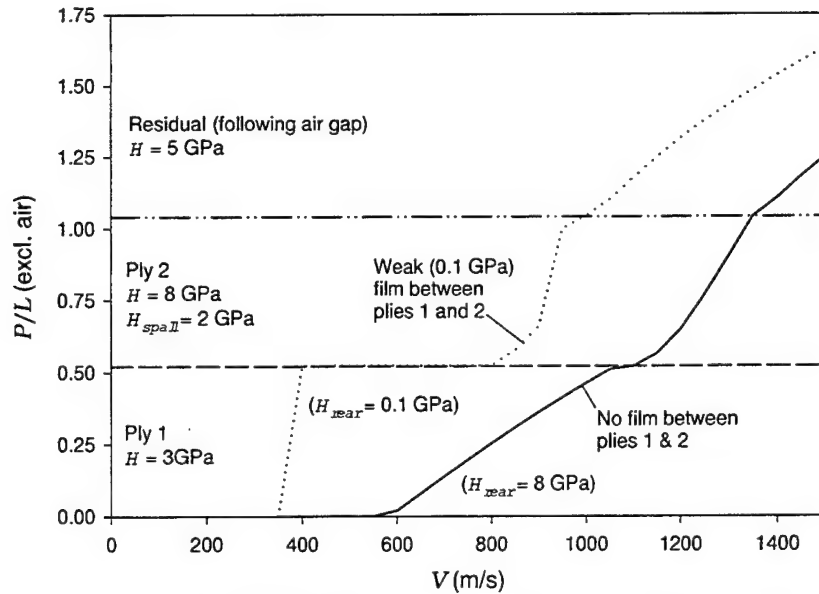| Plate No.	Thickness (mm)	ρ_T (g/cm^3)	H (GPa)	H_{SPALL} (GPa)	k_T
1	25	2.7	3	N/A	0.5
Interply	0.1	1.0	0.1	N/A	0.5
2	25	2.7	8	2	0.5
3 (air)	80	~0	0	N/A	0.5
4	∞	7.85	5	N/A	0.5

Figure 3. Effect of thin interply layer on FZ model.

in Figure 4 demonstrates this divergence clearly. It also shows how, once the second 25 mm ply is entered, the 8 GPa target resistance immediately drops below 6 GPa because of the influence of the subsequent air gap. One might infer that even the baseline case, without the interply film, is not modeled accurately, while the air gap is not yet detected in the first ply.

In fairness to the FZ model, it is true that these two examples have been chosen to accentuate the discrepancy between baseline and test cases. On the other hand, the intrinsic nature of the current FZ algorithm to handle only one interface at a time is a real and valid issue, regardless of the magnitude of the discrepancy for more "realistic" scenarios. And as cited previously, in the fully automated domain of ray tracing, thin target elements along shotlines will always remain a real possibility and should not become the cause for algorithm inaccuracy.

3. Basis for Modifications

The zone of influence in the target, ahead of the penetrator/target interface, which contributes to the effective target resistance, is a real phenomenon. Wright and Frank [5] examined the process by which the target response in this zone contributes to the target resistance. Others [6–8] have also studied this problem. This target zone of influence is generally recognized as the finite volume of target material undergoing deformation and is, in many models, approximated by the more readily
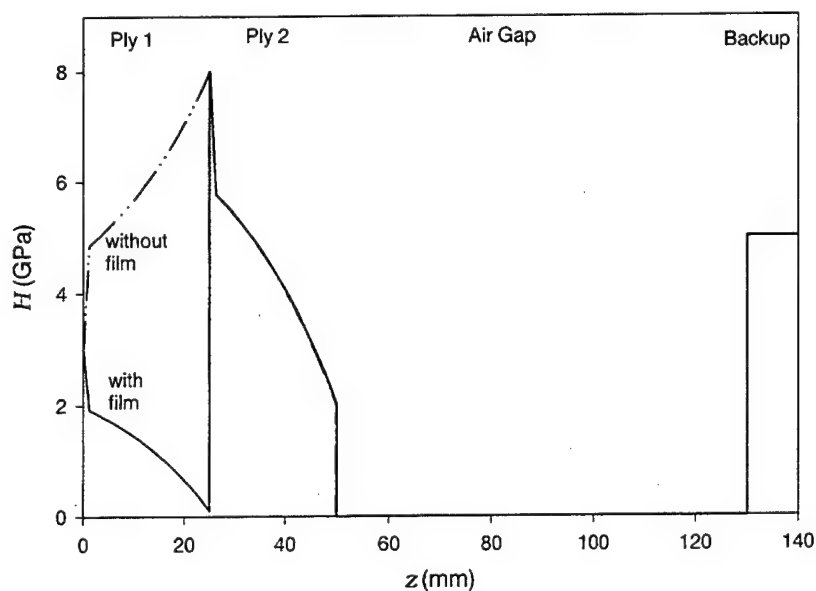
Figure 4. Influence of thin interply layer on FZ target resistance estimation.

6

identifiable zone of plastic deformation. With this latter physical interpretation, the zone of target plasticity ahead of the penetrator/target interface completely governs the effective resistance of the target. If this zone of plasticity were to extend across, for example, three target elements, then the effective target resistance would be composed of an appropriate combination of properties from each of those three layers. But, what combination of properties constitutes an appropriate one?

To address this question, the Walker-Anderson (WA) model [7] was explored for several reasons. First, it approximates the problem of integrating the target properties throughout the target's plastic zone into one of integrating the target properties along the axis of penetration. Though such a simplification could lose information about the lateral influence of target properties, it simplifies the mathematics considerably, while remaining wholly compatible with the framework of a TA or FZ model. Secondly, by assuming a particular profile for the flow field in the target's plastic zone, the WA model can analytically compute the exact stress and strain fields in the target's plastic zone that result from the assumed flow field. It is this resulting stress field that directly contributes to the evaluation of the effective target resistance. And, while it may be asserted that the assumed flow field of the WA model was selected for homogeneous target penetration, the approximation introduced by applying that flow field across material interfaces may be argued as reasonable and certainly preferable to ignoring the interface effects altogether. And as shown later, for the situation of a single interface within the target's plastic zone, the WA and FZ results are quite comparable.

Additionally, the WA model includes certain nonsteady inertial terms in the formulation that are not part of traditional TA or FZ methodology. In theory, accounting for nonsteady effects offers the ability to more accurately model the transient phases of the penetration process. Transient phases of penetration always occur at initial impact and during the final moments when the motion of a residual penetrator is arrested. For the impact of small L/D penetrators, a significant percentage of the total penetration event will occur in these transient stages. Furthermore, large transient gradients (*e.g.*, accelerations) can also arise when penetration transitions from one target element to the next. For targets comprising many elements, the net effect of these nonsteady terms could significantly affect the final result. And, for those cases where nearly steady-state penetration dominates the

7

penetration process (*e.g.*, long *L/D* penetrators into monolithic targets), these nonsteady terms lose significance, leaving the original underlying TA or FZ relations to govern.

4. Extent of Modifications

Though the WA model is distinct from FZ or TA methodology, there are naturally many parallels. Furthermore, the existing FZ methodology is known to accurately model ballistic penetration events, when the issues involving multiple material interfaces in the target's plastic zone are not germane. Whereas TA modeling is best suited to model the penetration of long rods into semi-infinite targets, the areas of FZ algorithm validity, based upon comparison to data [4], include long and short penetrators over a large impact-velocity regime against monolithic targets, as well as targets with "occasional" interfaces, accounting for the effects of target obliquity. Thus, given the generally exemplary performance of the existing FZ algorithm, there was little desire to "reinvent the wheel." The approach therefore adopted was an adaptation of those elements of the WA model into the existing framework of the FZ methodology, so as to enhance the existing capabilities, while leaving the FZ approach intact where possible. So, for example, those features of the WA model involving penetrator plasticity zones and wave speeds have not been utilized, since the existing FZ treatment of penetrators is excellent, albeit empirical [4]. And, though the FZ obliquity methodology could not be directly implemented in the WA framework, a very similar approach in the spirit of FZ was adapted.

Other aspects of the WA methodology, when utilized, were simplified for the sake of efficiency. For example, rather than using the rather complicated WA formulation to ascertain the lateral extent of plastic zone (from the crater centerline in terms of crater diameters, as a function of impact velocity), a simpler formulation was adopted. In particular, a closer examination of the behavior of the WA model reveals that, for a given material, the physical thickness of the plastic zone (from the crater wall, not the centerline) can be adequately approximated by a constant number of penetrator (not crater) diameters independent of impact velocity.

One aspect of the current modeling that is integral to neither the FZ nor WA models is the optional calculation of a time-dependent crater profile. In the case of FZ, crater-dimension computations are not part of the model. In the case of WA, because the formulation was developed

8

for homogeneous targets, the model formulation enforces a constant crater diameter throughout the penetration process for a given impact configuration. For the envisioned ARL application involving targets comprising multiple elements, such a limitation was not viable. Thus, two options are available in the proposed modeling: (1) crater radius is not explicitly calculated (but is implicitly treated as the rod diameter) and (2) a time-dependent crater radius is calculated, based approximately upon the notion that crater volume is proportional to the impacting kinetic energy. Option 1 provides the most compatibility with the existing FZ methodology since, in both cases, effects arising from lateral scale are keyed to the rod (and not the crater) diameter. Option 2, though requiring more calculation time, should (in some cases with multi-element targets) provide more accurate penetration modeling.[*] The proportionality between the crater volume and the kinetic energy is nominally the target resistance, and will be shown to match well to the data for tungsten and steel rods impacting RHA [7, 9]. The availability of a crater profile prediction may also, in the future, assist SLAD in their V/L assessment of terminal-ballistic events.

Because the WA model was originally presented for monolithic targets, a novel adaptation was required in order to apply it to laminated and/or finite targets. Because the WA model, as derived [7], pertains to only semi-infinite targets, the evaluated stress integrals that it presents cannot be directly employed in the proposed solution strategy, when the plastic zone ahead of the rod/target interface extends into more than one target element or to a free surface. To circumvent this limitation, the WA integrals are dynamically re-evaluated at each integration step, using the limits of spatial integration corresponding to each successive target element in the entrained plastic zone, and are solved for the normal-stress difference across each respective target element. By adding the integral contributions for normal-stress difference across all the target elements, the stagnation stress at the rod/target interface is reconstituted. The summation of terms constituting this stress signify contributions from each affected target element towards the aggregated inertial (ρU^2), target resistance (R_T), and nonsteady (d/dt) terms.

---

[*]The (radial) size of the crater affects the rate and manner in which the flow field decays from the rod/target interface, thus affecting the target-resistance formulation and the (axial) penetration rate. Also, the axial penetration equations include dR/dt terms not part of the original WA formulation.

5. Algorithmic Details

5.1 Extent of Plastic Zone. In WA modeling, target properties are formulated by way of an integration process through the plastic zone in the target, located ahead of the rod/target interface. The extent of this zone is characterized by a nondimensional, velocity-dependent model parameter, α. Though the crater formed via the WA model is roughly cylindrical, the leading edge of the crater (at the rod/target interface) has a hemispherical cap of crater radius R. The length αR defines the distance from the radial center of the hemispherical crater cap to the outer fringes of the target's plastic zone. The actual thickness of the plastic zone, therefore, as measured from the edge of the hemispherical crater, is $(\alpha-1)R$. Figure 5 depicts some of the relevant geometrical parameters.

In the WA model, a complicated formulation was developed to relate the value of this α parameter to the penetration rate through the target. A simpler alternative was sought and found, applicable over a wide range of conditions. Simply put, the thickness of the plastic zone may be approximated as a constant for a given target element; namely, $R(\alpha - 1) = constant$. The constant may be *a priori* specified as a material parameter, "plastic-zone thickness," for each target element. By specifying this plastic-zone thickness as a multiple of rod diameters, as in ξD, for example, not only is ξ made nondimensional, but it may be readily related to the low-velocity limiting value for α, namely α_0. In this limiting case, the crater radius R approaches the rod radius $D/2$, and the value for α_0 may thus be related to ξ, as $\xi = (\alpha_0 - 1)/2$.
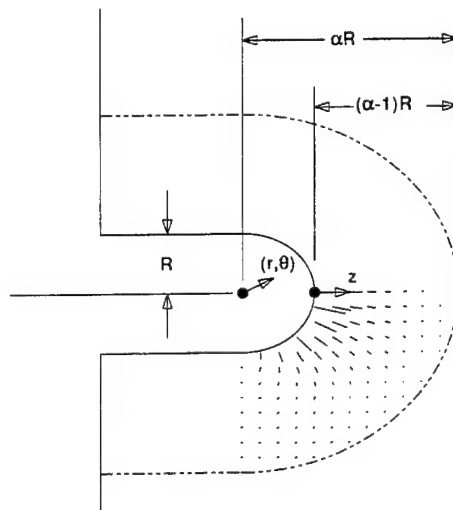

Figure 5. Description of the target's plastic zone in the WA model [8].

To test the reasonableness of the hypothesis that the plastic-zone thickness is independent of penetration velocity, examine the case of a tungsten long rod penetrating an RHA target and compare it against the α vs. U curve presented by Walker and Anderson [7]. To obtain quantitative values for α using this hypothesis, values for R must be known. The empirical fit of Bjerke *et al.* [9] presents the crater to rod diameter ratio as a function of striking velocity, V_0 (km/s), as

$$2R/D = 1.1524 + 0.3388 \cdot V_0 + 0.1286 \cdot V_0^2 \ . \tag{2}$$

Bjerke's curve had been fit to data over the range of V_0 from approximately 1 to 4.5 km/s. In order to express the result in terms of α vs. U, as did Walker and Anderson [7], the striking velocity V_0 must be related to the penetration velocity, U. For purposes of this comparison and for the sake of simplicity, relate these quantities through the hydrodynamic relation, $V_0 = (1 + \gamma^{1/2})U$, where γ is the target to rod density ratio ρ_T/ρ_R equal to 0.4508 in the case of tungsten on steel.

The comparison may now be presented in Figure 6 and is very good, except at the lowest of velocities, where it is nonetheless adequate. The simplicity of the assumption $R(\alpha - 1) = \xi D$ makes for a greatly streamlined implementation, with many fewer material parameters and computational steps than the original WA formulation. In Figure 6, the case of $\alpha_0 = 8.9$, for example, corresponds to a plastic-zone thickness of 3.95 rod diameters.
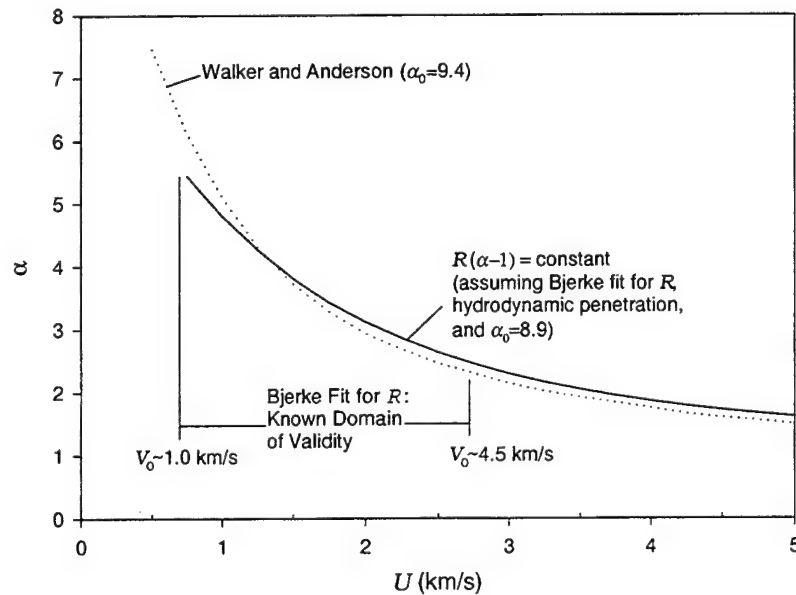

Figure 6. Comparison of Walker and Anderson fit to the constant $R(\alpha-1)$ assumption [7].

11

A rational explanation for the reasonableness of the constant plastic-zone thickness assumption is surmised. Namely, for a given target strength, the work required to infinitesimally expand a crater from radius R to $R + dR$ should be approximately proportional to the crater-wall area, over which the crater-growth pressure is applied, times the applied pressure. At the hemispherical tip of the newly forming crater, this area grows with crater size as R^2. The required pressure, according to WA theory, grows roughly with $\ln(R/D)$, so that work required goes as $R^2 \ln(R/D)$. Correspondingly, given the assumed constant-thickness plastic zone, the volume of entrained plastic material in the hemispherical cap grows roughly as R^3 for $R{\sim}D$, while approaching R^2 for $R{>>}D$. Thus, the increment of plastic-strain energy to grow the crater size, being roughly proportional to the plastic-zone volume, also grows approximately with R^3 to R^2 functional behavior. Because the $R^2 \ln(R/D)$ function also grows as R^3 for $R{\sim}D$, while approaching R^2 for $R{>>}D$, it follows that both the work required for and the plastic strain energy that results from an infinitesimal expansion of the crater are roughly of the same functional form and thus approximately proportional to each other. This conclusion follows merely by assuming a plastic zone of constant thickness.

As a result of adopting the $R(\alpha - 1) = constant$ assumption, not only is the dynamic value of α obtainable when the time-dependent value of R is known, but the rates at which R and α vary are coupled as well. A simple differentiation of the assumption gives the relation by which the derivatives may be interrelated:

$$\dot{R}(\alpha - 1) + \dot{\alpha} R = 0 \quad . \tag{3}$$

5.2 Numerical Integration Approach. In the FZ methodology, penetration velocity U and rod velocity V are algebraically tied through the modified Bernoulli equation,

$$k_P \rho_P (V - U)^2 + Y = k_T \rho_T U^2 + H \quad , \tag{4}$$

where k_P and k_T are the penetrator and target "shape factors" of Alekseevskii [3]; ρ_P and ρ_T are the rod and target densities; and Y and H are the rod strength and target resistance, respectively. Thus, under FZ, the separate integration of one of them (typically V via the rod deceleration equation) was sufficient to algebraically determine the other (U). In the current modeling, however, the nonsteady Bernoulli equation (representing the force-momentum balance along the centerline) is a function of

12

not only U and V, but also their time derivatives dU/dt and dV/dt. Thus, while V is integrated by way of the rod deceleration equation

$$\dot{V} = - \frac{Y}{\rho_P (L-s)} \tag{5}$$

(L being the rod length, and s being the rod's plastic-zone thickness), U must be independently obtained from the nonsteady Bernoulli equation [8] by isolating dU/dt and integrating. It is shown here, applied to the WA flow field for long-rod penetration:

$$\left(k_P - \frac{1}{2} \cdot \frac{\dot{s}}{L} \right) \rho_P (V-U)^2 + Y - \frac{\rho_P s}{2} (\dot{V}+\dot{U}) = k_T \overline{\rho} U^2 + \overline{H} + X_U \frac{\dot{U}}{U} + X_\alpha \frac{\dot{\alpha}}{\alpha} + X_R \frac{\dot{R}}{R} \;. \tag{6}$$

On the target side of the equation, $\overline{H}$, $\overline{\rho}$, X_U, X_α, and X_R are time-dependent quantities integrated through the plastic zone of the target. If the plastic zone in the target spans several target elements, the values taken on by these parameters are summations of properties from all constituent target elements, as described in section 5.5. However, if the target's plastic zone comprises a single target element only, then the values taken on by these terms are simplified greatly, expressible as

$$\overline{\rho} = \rho_T \;, \tag{7}$$

$$\overline{H} = H \;, \tag{8}$$

$$X_U = \rho_T U R (\alpha-1)/(\alpha+1) \;, \tag{9}$$

$$X_\alpha = 2\rho_T U R \alpha /(\alpha+1)^2 \;, \text{and} \tag{10}$$

$$X_R = \rho_T U R (\alpha-1)/(\alpha+1) \;. \tag{11}$$

Regardless of the actual evaluation of these parameter values, the nonsteady Bernoulli equation (6) shows their generic interrelation. In the actual implementation currently suggested, several simplifications have been made to this equation. First, because of the excellent functionality provided by the existing FZ treatment of the penetrator [by empirically treating $Y = Y(L)$], the plasticity associated with the rod is currently neglected, by treating both s and ds/dt as negligible quantities. Future treatments may revisit this simplification. Furthermore, the quantities $d\alpha/dt$ and dR/dt, independent in the nonsteady Bernoulli equation, are herein treated in a coupled manner [via equation (3)], an assumption detailed in section 5.1.

13

Though an optional capability to model the crater radius is described in section 5.3, the equations derived to this point may nonetheless be solved by assuming a constant crater diameter (*i.e.*, $R = D/2$). To retain maximum compatibility with the FZ algorithm, which bases its interelement transition dimension upon the rod diameter, the constant-crater-diameter mode of the revised algorithm will employ the rod diameter itself as the (constant) crater diameter. When this is done, dR/dt and thus $d\alpha/dt$ terms [via equation (3)] are identically zero. When employing this mode for the case of monolithic penetration, and in conjunction with neglecting s and ds/dt, equation (6) differs from equation (4) by only the $X_U/U \cdot dU/dt$ term.

Whereas equation (4) is algebraic, equation (6) remains differential, despite the aforementioned simplifications, and therefore continues to require numerical integration. However, for monolithic penetration, where the penetration velocity U changes slowly except for the onset and final moments of penetration, one would expect the dU/dt term to carry only small significance. As such, the revised (WA-based) algorithm [employing equation (6)] should, for this impact condition, closely match the results of the FZ algorithm [employing equation (4)]. Figure 7 shows this comparison for the cases of $L/D = 3$ and 30 tungsten rods penetrating RHA. In both models, a 5 GPa target resistance was employed. The revised algorithm requires a plastic-zone-thickness parameter specification (section 5.1), taken in the present case as 3.75 rod diameters. The only input difference between the corresponding FZ- and WA-based simulations was the rod strength, which was taken as 1.9 GPa in the FZ formulation and 1.8 GPa in the WA-based formulation.

5.3 Crater-Radius Calculation. The calculation of a time-dependent crater radius has been implemented as an option into the proposed methodology, though it is not part of either the FZ or WA models. Crater radius does have a secondary effect on the axial penetration equations. This effect is more pronounced at obliquity, where the expanding crater may reach a target/target interface prior to the arrival of the rod itself. Additionally, the accurate knowledge of the crater dimensions may provide valuable data for subsequent V/L modeling.

The basic premise of the crater-modeling algorithm is the assumption that the crater volume displaced is proportional to the impacting kinetic energy. While this assumption has frequently
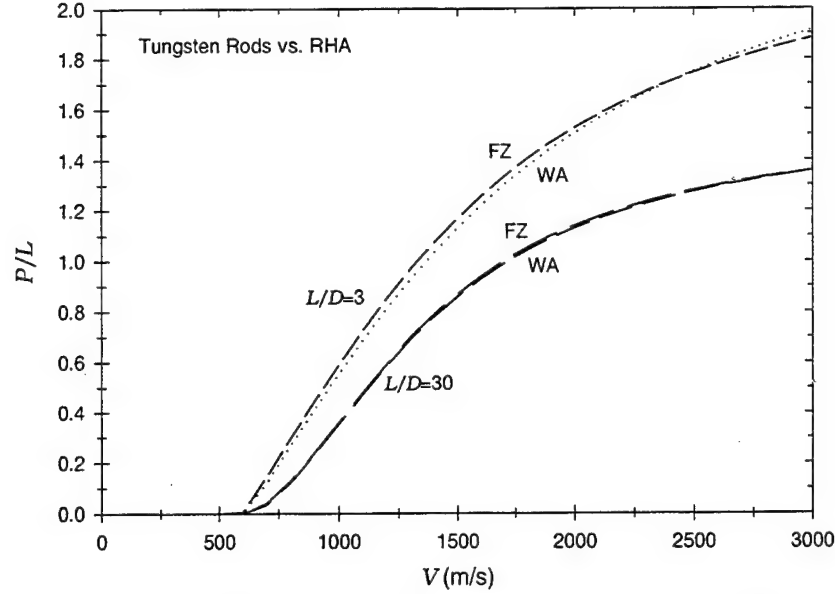
14

Figure 7. Nondimensional Penetration vs. Velocity for original (FZ) and revised (WA) models for semi-infinite penetration.

been employed in the crater modeling of small L/D impacts, or even the case of particulated shaped-charge jet penetration, an adaptation was required for the case of continuous long-rod penetration. In this case, the *rate* of energy deposition (per unit depth penetration) by the rod is made proportional to the *rate* of crater-volume creation, the proportionality being nominally proportional to the effective radial target resistance H_R. Implicit in this analysis is the assumption that both rod and target are eroding. The special cases of rigid rod and target are addressed at the end of this section.

Energy is delivered to the target by the rod in the form of both force over distance (work) as well as specific KE of eroding rod delivered to the rod/target interface:

$$H_R \frac{d(Vol)}{dP} = \frac{dE_K}{dP} + \frac{dW}{dP} \quad . \tag{12}$$

By taking the control-volume boundary for energy delivered by the rod to be the onset of the rod's plastic zone, the undeformed dimensions, velocities, and properties of the rod may be used in the energy balance. The crater volume per depth of penetration $d(Vol)/dP$ is the crater's area πR^2, with R being the sought-after variable of this exercise. The rate at which usable kinetic energy is delivered to the target per unit depth of penetration is better understood as $dE_K/dP = dE_K/dL \cdot (dL/dP)_{eff}$, the kinetic energy of the rod per unit length times the (effective) rate

15

at which rod length is consumed in the form of penetration. The specific kinetic energy per unit length of rod dE_K/dL is simply $1/2 \cdot \rho_P V^2 (\pi D^2 /4)$. Finally, the rate of external work done by the rod dW/dP is just the force applied by the rod $Y_0 (\pi D^2 /4)$. Combining these expressions provides the following result:

$$R = D/2 \cdot \left\{ [\tfrac{1}{2} \rho_P V^2 (dL/dP)_{eff} + Y_0] / H_R \right\}^{1/2} \quad , \text{when } 0 < U < V. \tag{13}$$

In no event is R permitted to be less than $D/2$.

The target resistance offered for radial crater formation H_R will generally be identical to that offered against axial penetration $\overline{H}$. However, near the rear of a target element, the axial resistance can and does fall off drastically if that rear surface is a free surface. In contrast, however, the ability to resist radial crater growth will, at most, fall off to the level of the material's yield strength. Thus, H_R is taken as max(Y_T, $\overline{H}$). Based on elements of WA theory, the target element's yield strength Y_T may be approximated, in terms of target resistance H and other known parameters, as $Y_T = 3/7 \cdot H / \ln(\alpha_0)$, where α_0 is related to the target element's plastic-zone thickness, as described in section 5.1.

The instantaneous rate at which rod length is consumed per unit of penetration dL/dP is kinematically related to velocities V and U as $dL/dP = (V - U)/U$. For two reasons, however, this precise value of dL/dP may not be that taken as the effective value $(dL/dP)_{eff}$ used in the crater radius calculation. First, there does not in reality exist a one-to-one relation between an infinitesimal increment of penetration and the resulting value of crater diameter. Allowances need to be made during moments of penetration transient (especially at penetration onset), when the instantaneous dL/dP can far exceed its steady-state value. At these moments, it is not reasonable to expect a small transient section of the crater to have an excessively large diameter compared to the adjacent crater profile. The expedient remedy adopted has been to cap the maximum allowable value of $(dL/dP)_{eff}$ (in this crater-radius calculation only) to a value related to the hypothetical steady-state (not instantaneous) erosion rate.

The theoretical value for steady-state dL/dP is obtained by solving, in terms of V, for the quantity $(V - U)/U$ in the steady-state, modified Bernoulli equation:

16

$$1/2\,\rho_P(V-U)^2 + Y_0 = 1/2\,\overline{\rho}U^2 + \overline{H} \quad . \tag{14}$$

However, the allowable cap on $(dL/dP)_{eff}$ is modified *ad hoc*, from this steady-state value of dL/dP, consistent with the experimental record on crater size, and is denoted by max$(dL/dP)_{eff}$. The result, in terms of V, depends on whether the rod and averaged target densities are equal. In the case that they are equal and $\gamma = \overline{\rho}/\rho_P = 1$,

$$\max(dL/dP)_{eff} = (1+x)/(1-x) \quad , (\gamma = 1), \tag{15}$$

where

$$x = 0.5(\overline{H} - Y_0)/(\tfrac{1}{2}\rho_P V^2) \quad . \tag{16}$$

Note that, except for the leading 0.5 multiplier in the definition of x, this result represents the exact solution to the modified Bernoulli equation for $(V-U)/U$. The 0.5 multiplier, however, is an *ad hoc* modification to the theoretical steady-state result, chosen to facilitate a fit to steel-on-steel crater-profile data [7]. For the case of unlike densities, where $\gamma \neq 1$, the result is

$$\max(dL/dP)_{eff} = (-\gamma + \sqrt{x})/(1 - \sqrt{x}) \quad , (\gamma \neq 1), \tag{17}$$

where x is now defined as

$$x = \gamma + 0.4(1-\gamma)(\overline{H} - Y_0)/(\tfrac{1}{2}\rho_P V^2) \quad . \tag{18}$$

Like the $\gamma = 1$ case, the only *ad hoc* modification to the theoretical result is the introduction of a multiplier (in this case, 0.4) in the definition of x. The selection of the 0.4 multiplier results in good correlation to tungsten-rod on RHA-target crater-profile data fit by Bjerke *et al* [9]. Figure 8 shows these correlations to other fits [7, 9] for both steel on steel ($\gamma = 1$) and tungsten on steel ($\gamma \neq 1$).

Though there appears to be ample opportunity for max$(dL/dP)_{eff}$ to be negative or undefined, the mathematical nature of the steady-state penetration equations actually precludes it, when both the target and rod are eroding. In those limiting end states of rigid-target and rigid-rod penetration, special provisions are taken. In the case of rigid-target rod erosion, the crater size is inconsequential, since there is no incremental growth of the crater. In the case of rigid-body penetration, there is no kinetic energy flux that would result from a feeding of rod into the stagnation zone, since rod material does not feed into the stagnation zone. Consequently, look merely to the plastic work done on the target by the actual rod/target interface stress. Since the rod is rigidly penetrating, this interface stress is less than the yield strength Y of the rod. However, the
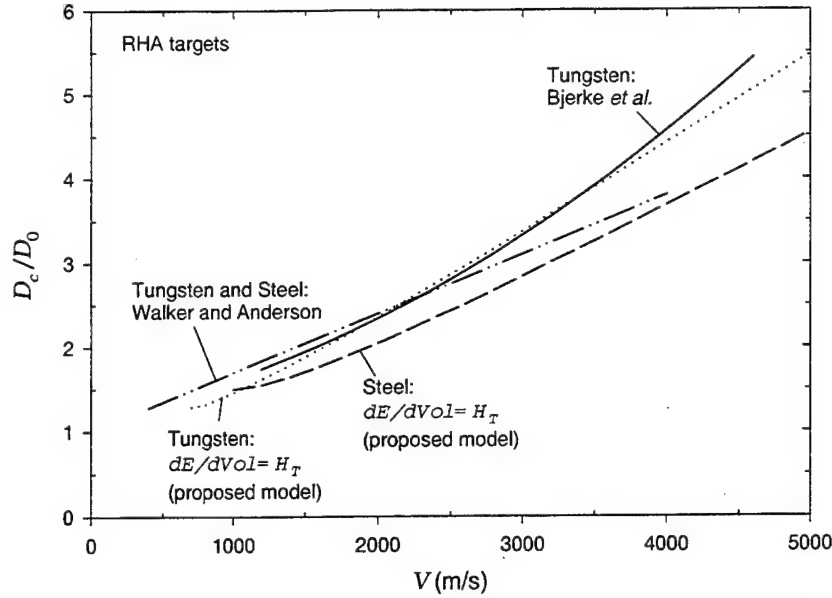
Figure 8. Comparison of proposed crater-diameter modeling with fits from other models [7, 9].

(steady-state) magnitude of this interface stress may be obtained from the flow kinematics of the target. Balancing the work of this applied stress with the implied crater volume (as per the original energy/crater-volume proportionality assumption) gives

$$R = D/2 \cdot \sqrt{[1/2\,\rho_T U^2 + \overline{\overline{H}}]/H_R} \quad , \text{(when } U = V). \tag{19}$$

A final aspect of the proposed cratering methodology at variance with that already described is the treatment the crater-profile development in the final transient stage, as the ballistic event concludes. Empirical experience indicates that an established flow pattern does not cease instantaneously and that the bottom of a penetration channel will tend to retain a pseudohemispherical shape because of flow-field inertia. To this end, at the moment when the crater radius begins decreasing within a target element, current values of R and U are noted as "critical" values. Subsequent crater radius is developed according to the following *ad hoc* relationship:

$$R = D/2 + (R_{crit} - D/2)\sqrt{1 - (1 - U/U_{crit})^2} \quad , \text{(when } dR/dt < 0). \tag{20}$$

This form is obeyed for the decay of crater radius until such time that either R as described by the standard method would indicate that $dR/dt \geq 0$ or a new target element is entered. In either of these cases, the "critical" values of R and U are reset and the standard calculation method prevails. This

18

form has the crater radius diminishing from R_{crit} to $D/2$ as the penetration velocity falls from U_{crit} to zero.

5.4 Nonsteady Terms. The original WA model does not provide for a varying crater radius and, as such, does not incorporate radial variation (dR/dt) terms into its formulation. Rather, nonsteady terms in WA methodology are limited solely to unsteady penetration rate (dU/dt) and extent of plasticity ($d\alpha/dt$) terms. Thus, the introduction of dR/dt quantities into the governing force-momentum balance equation (section 5.2) is an extension beyond the scope of the original WA model. This extension will only play a role if the variation of crater radius over time is modeled. In this proposed implementation, the choice to dynamically model crater radius is an option left to the discretion of the model user.

5.5 Piecewise Integration of Momentum. Discussion of the momentum equation to this point has largely centered upon the effect of including nonsteady penetration terms as an extension to the FZ methodology. These nonsteady effects, though brought about naturally to small degree in the course of penetrator deceleration, may play a larger role when the unsteadiness of the penetration event is purposefully induced via time fluctuations in the penetration (*i.e.*, rod/target interface) velocity. In addition, however, to unsteady terms that are introduced as a direct result of interface fluctuations (*i.e.*, terms proportional to time rates of change of the kinematic variables U, R, and α), the "effective" target material properties themselves (*i.e.*, H and ρ) change as target/target interfaces become entrained within the plastic zone that leads the rod/target interface.

Though theories like Wright-Frank [5] and WA [7] assert that the plastic zone ahead of the rod/target interface is responsible for the makeup of the target-resistance terms, neither analysis addresses the situation of a multi-element target. The existing FZ methodology, on the other hand, does permit this feature to be modeled in a limited way. While no provisions are made by FZ to aggregate density into an "effective" value, the transition in effective target resistance, in advance of an interface, is modeled to change exponentially from the original value to the value of the succeeding element, reaching the new element's resistance just as the penetration interface reaches the new target element. The growth (or decay) exponent is proportional to the remaining distance between the rod/target and target/target interface, normalized by the rod diameter. However, this

19

modeling approach, as implemented, accounts for the resistance of the next target element only, regardless of whether subsequent elements may also be entrained in the target's plastic zone.

While the WA methodology [7] in no way addresses the issue of a plastic zone that extends across a target/target interface, a methodology may be inferred based on the WA framework with the use of a single additional assumption; namely, that the hemispherical displacement field posited by WA methodology is assumed to remain valid, even as that displacement field spans across multiple target elements. While such an assumption can never be strictly accurate, it is believed that the errors introduced by it are of secondary importance.

When the displacement field governing the target's plastic zone is known, the axial centerline momentum integral [extended Bernoulli equation (9)] may be evaluated. However, because the extended Bernoulli equation has material density within the integrand of the stress integrals [8], the evaluation is straightforward only when the limits of integration span a region of constant density. A full integration across a plastic zone comprising multiple target elements implies a series of piecewise integrals over individual target elements. The piecewise integral (*i.e.*, across a single target element of constant density) may be evaluated for the normal-stress difference across the element. For the problem of long-rod penetration, this integral across target element i (ranging from $z = z_1$ to z_2) becomes

$$\sigma_{zz}\big|_{z_1}^{z_2} = k_T \rho_{Ti} V_z^2 \big|_{z_1}^{z_2} + 2\int_{z_1}^{z_2} \sigma_{xz,x}\,dz + \rho_{Ti}\int_{z_1}^{z_2} \frac{\partial}{\partial t}\big(V_z + U\big)\,dz, \qquad (21)$$

where the z coordinate of integration coincides with the position of the target element along the axis of symmetry (centerline) of the penetration and V_z is the axial component of the material velocity field. Both z and V_z are measured relative to the moving rod/target interface. When the specific WA flow field is assumed, the velocity field is known and the associated stress field may be inferred, thus allowing the required integrals to be evaluated. For a target element that falls within the target's plastic zone, and whose location along the shotline spans from $z_1 = (\beta_1 - 1)R$ to $z_2 = (\beta_2 - 1)R$, the extended Bernoulli integral over that target element gives the following:

$$\sigma_{zz}\big|_{z_1}^{z_2} = \frac{\alpha^4}{(\alpha^2-1)^2}\left[\frac{(2\beta_1^2-1)}{\beta_1^4}-\frac{(2\beta_2^2-1)}{\beta_2^4}\right]k_T\rho_{Ti}U^2 \;+\; \frac{\ln(\beta_2/\beta_1)}{\ln(\alpha)}H_i$$

$$+\; \frac{\rho_{Ti}R}{(\alpha^2-1)}\left[\frac{(\beta_1^2+\alpha^2)}{\beta_1}-\frac{(\beta_2^2+\alpha^2)}{\beta_2}\right]\dot{U} \;+\; \frac{2\rho_{Ti}R\alpha}{(\alpha^2-1)^2}\left[\frac{(\beta_2^2+1)}{\beta_2}-\frac{(\beta_1^2+1)}{\beta_1}\right]U\dot{\alpha} \qquad (22)$$

$$+\; \frac{\rho_{Ti}\alpha^2}{(\alpha^2-1)}\left[\frac{(2\beta_1-1)}{\beta_1^2}-\frac{(2\beta_2-1)}{\beta_2^2}\right]U\dot{R} \quad.$$

If this target element i were to completely span the plastic zone of the target, corresponding to $\beta_1 = 1$ and $\beta_2 = \alpha$, this normal-stress difference would correspond to the stagnation stress and would exactly reduce to the target side of equation (6) as presented in section 5.2; namely, yielding equations (7)–(11).

In the general case, however, where the target's plastic zone comprises several target elements, normal-stress continuity at target-element interfaces dictates that the total normal-stress difference across the target may be ascertained by summing the stress difference across each successive target element, until the far fringes of the target's plastic zone have been reached. Because the stress at any point beyond the target's plastic zone is zero in WA methodology, the total stress difference thus evaluated represents the magnitude of the stagnation stress at the rod/target interface.

One may therefore generalize the specification of the target terms, when referring back to equation (6). In particular, for a plastic zone that spans across target elements ranging from element m to n, one obtains the following generalized expressions for the target parameters:

$$\bar{\rho} = \sum_{i=m}^{n}\frac{\alpha^4}{(\alpha^2-1)^2}\left[\frac{(2\beta_i^2-1)}{\beta_i^4}-\frac{(2\beta_{i+1}^2-1)}{\beta_{i+1}^4}\right]\rho_{Ti} \quad, \qquad (23)$$

$$\bar{H} = \sum_{i=m}^{n}\frac{\ln(\beta_{i+1}/\beta_i)}{\ln(\alpha)}H_i \quad, \qquad (24)$$

$$X_U = UR\sum_{i=m}^{n}\frac{\rho_{Ti}}{(\alpha^2-1)}\left[\frac{(\beta_i^2+\alpha^2)}{\beta_i}-\frac{(\beta_{i+1}^2+\alpha^2)}{\beta_{i+1}}\right] \quad, \qquad (25)$$

$$X_\alpha = UR\sum_{i=m}^{n}\frac{2\rho_{Ti}\alpha^2}{(\alpha^2-1)^2}\left[\frac{(\beta_{i+1}^2+1)}{\beta_{i+1}}-\frac{(\beta_i^2+1)}{\beta_i}\right] \quad, \text{and} \qquad (26)$$

21

$$X_R = UR \sum_{i=m}^{n} \frac{\rho_{Ti} \alpha^2}{(\alpha^2 - 1)} \left[\frac{(2\beta_i - 1)}{\beta_i^2} - \frac{(2\beta_{i+1} - 1)}{\beta_{i+1}^2} \right] . \qquad (27)$$

The limits $\beta_m = 1$ and $\beta_{n+1} = \alpha$ apply in all cases [recall that $\beta_i = 1 + (z_i/R)$], corresponding to the geometric limits of the plastic zone [$i.e.$, $0 \leq z \leq (\alpha - 1)R$], with β_i values for target elements between m and $n + 1$ falling numerically between values of 1 and α, depending upon their relative location within the plastic zone.

With equations (23)–(27), the extended Bernoulli equation (6), now has the means to more accurately characterize the influence of thin target elements upon the effective target resistance and density, as well as the nonsteady terms of the momentum balance. As such, the two example problems cited as the motivation for pursuing these revisions to the existing FZ methodology may be revisited. It was first confirmed that the revised algorithm provided nominally identical results when comparing the test case to the corresponding baseline. This confirmation indicates that the revised algorithm is insensitive to the mere presence of thin-layer interfaces.

The next comparison is to the results of the original FZ methodology (in particular to the baseline-case FZ results, which do not suffer from the thin-ply deficiencies). For the problem earlier cited as Example 1, Figures 9 and 10 provide the comparison. Not only can the revised algorithm (WA) match the original FZ result for penetration vs9. velocity (Figure 9) but the functional decay of target resistance through the thickness of the target, denoted "WA (Plastic Zone = 4.3D)" and corresponding to equation (24), correlates excellently with the exponential decay form of the FZ model. However, whereas the FZ form is only properly computed if the target comprises a single 50 mm plate, the WA result displayed is that obtained for both a 50 mm plate, as well as a 48 + 2 mm multiplate configuration. For the revised (WA) simulations, all simulation parameters were identical to those employed in the corresponding FZ simulations (see Table 1). Additionally, the WA simulations were run in constant-crater-diameter mode, with a plastic-zone thickness of 4.3 rod diameters. Figure 10 also includes, for purpose of illustration, the revised model's target resistance when the plastic-zone extent is taken as 3.5, rather than 4.3, rod diameters. The difference from the 4.3 curve shows the extent to which the effective target resistance is affected by designated changes in the size of the plastic zone.
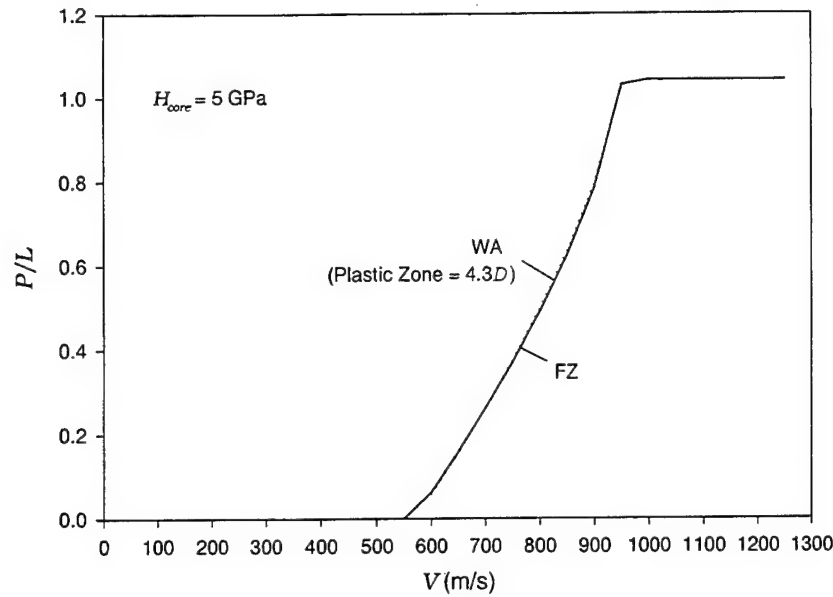
Figure 9. Example 1: Normalized Penetration vs. Velocity for FZ and revised (WA) models.
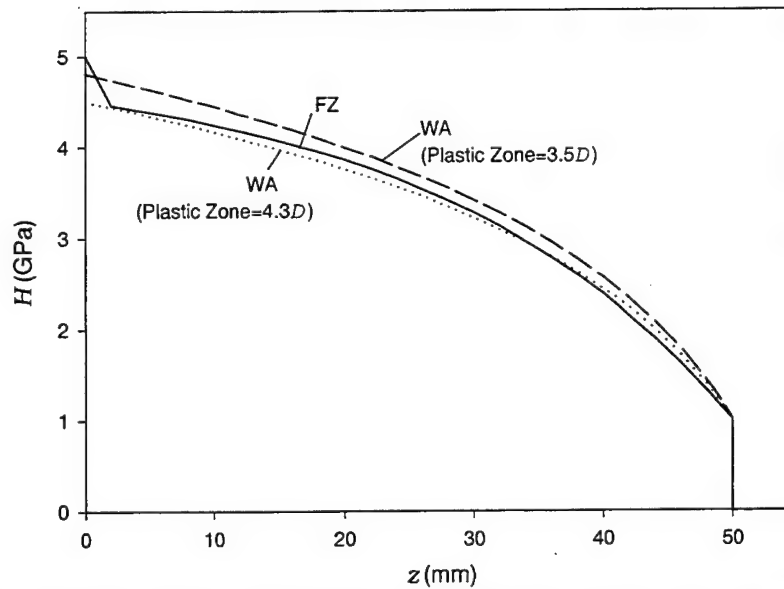

Figure 10. Example 1: Target Resistance vs. Location for FZ and revised (WA) formulations.

To compare now the revised model to the problem cited in section 2 as example 2, results are presented in Figures 11–12. The FZ results presented correspond to the baseline case, without the thin-interply film between the soft and hard plies of the target, whereas the revised (WA) results are independent of the presence of the interply film. Though the revised (WA) formulation compares more closely to the FZ baseline (in Figure 11) than did the FZ test case
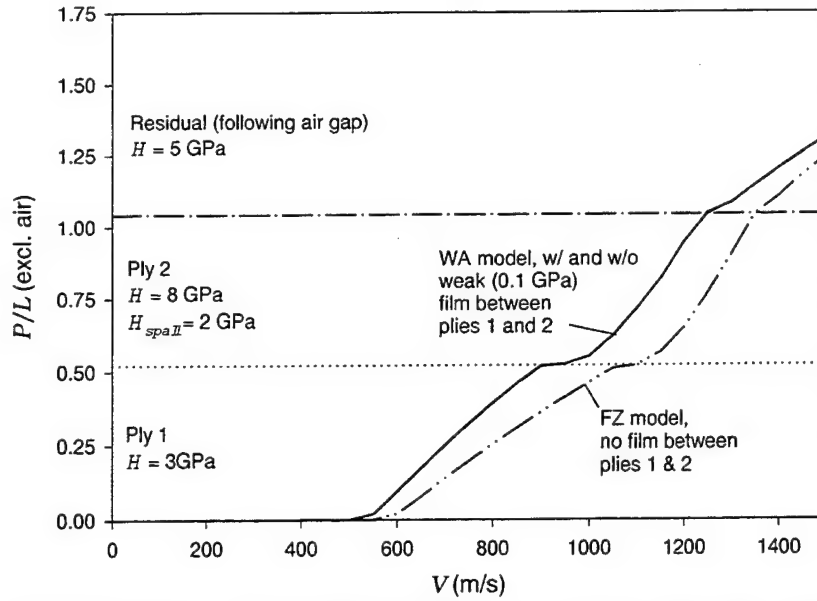
23

Figure 11. Example 2: Normalized Penetration vs. Impact Velocity for FZ and revised (WA) formulations.
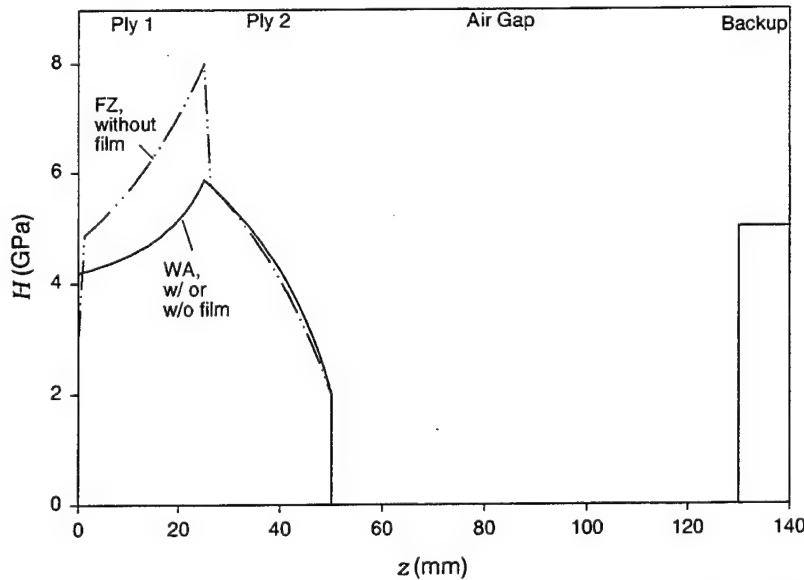
Figure 12. Example 2: Target Resistance vs. Location for FZ and revised (WA) formulations.

with thin interply film (in Figure 3), there is still some discrepancy evident in Figure 11. The source of this discrepancy may be gleaned from the target-resistance plot in Figure 12. Even without the thin-interply film that demonstrated (via the example 2 test case) the inability of FZ methodology to perceive more than one target interface in advance, the baseline case itself, to a lesser extent, is subject to the same deficiency. In particular, the FZ baseline fails to detect the

24

rear surface of the second target ply, until actually in that ply. As such, the target resistance in the first ply rises fully to 8 GPa at the ply-1/ply-2 interface before suddenly detecting a loss of strength originating from the free surface of ply 2. By contrast, the revised (WA) formulation avoids sudden internal changes in target resistance (and other properties) by employing the plastic-zone integration process embodied in equations (23)–(27). For a sense of scale, note from Table 2 that the thickness of ply 1 and ply 2 are each about 1.5 D. A final note on these WA simulations is that they were performed in constant-crater-diameter mode, with a plastic-zone extent of 4.0 D.

5.5.1 Obliquity Considerations. The presence of target obliquity complicates the problem of integrating piecewise across multiple target elements. The reason for this complication arises from the fact that the integration technique employed in the current algorithm is that of a line integral along the shotline. A consequence of reducing the kinematics of a three-dimensional (3–D) penetration event to a line integration is that the presence of obliquity guarantees that subsequent target elements will become laterally entrained within the target's 3–D plastic zone prior to becoming entrained along the shotline itself (see Figure 13). If no special provisions are made, this lateral entrainment will not be detected by the line-integration algorithm and the effect of target obliquity will reduce merely to increased line-of-sight thickness.
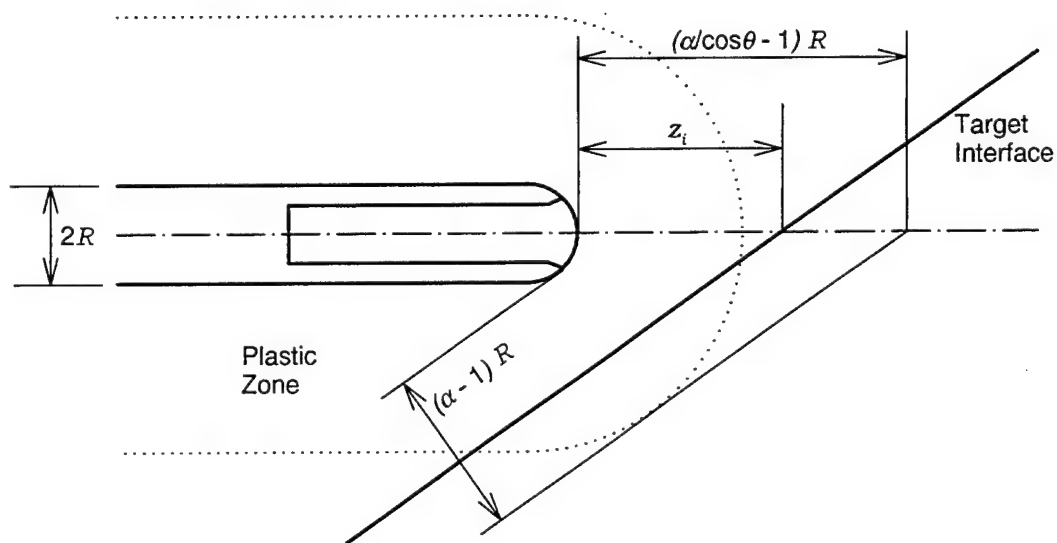

Figure 13. Geometrical considerations associated with oblique penetration.

25

The technique adopted, though not identical to, is in the flavor of the FZ approach to the obliquity problem. In the FZ algorithm, which allows for a smooth transition in target resistance properties over a finite distance, the exponent that governs that transition is proportional to the normal distance between the rod/target and target/target interfaces. Also, because of the hemispherical nature of the plastic-zone cap, the WA model would likewise indicate that the ability of a remote target element to influence the aggregated target properties should be determined by the normal distance from the wall of the crater to the target/target interface in question.

Therefore, in order to retain the basic numerical approach of employing a 1–D integration along the shotline dimension, the axial location of interfaces and extent of plastic zone are transformed as a function of obliquity, by projecting the extent of the plastic zone perpendicular to the target normal onto the axial line-of-sight. Using the transformation variable

$$M = \frac{\alpha - 1}{(\alpha / \cos\theta) - 1} \quad , \tag{28}$$

where θ is the target obliquity measured from surface normal, the extent of plastic zone (as projected onto the shotline) may be seen to span from $0 \le z \le (\alpha - 1)R/M$, with the intermediate target/target interfaces being defined by $\beta_i = 1 + (z_i M/R)$. With this transformation variable M (which equals unity at zero obliquity), a target element will begin to influence the aggregated target properties as soon as any part of the plastic zone overlaps the affected target element.

For the case of a simple target plate at obliquity, the results of this methodology may be compared with the FZ model, which is wholly adequate for this class of problem. Figures 14–16 depict residual length, residual velocity, and nonperforating penetration, as a function of obliquity, for a 1250 m/s impact of an $L/D = 3$ tungsten penetrator (same as in examples 1 and 2) into a hard ($H = 5$ GPa), 50 mm ($t/D = 1.04$) aluminum plate. The WA simulations were performed in variable crater-diameter mode, with a plastic-zone-extent of 3.5 D. The similarity of results indicates that the current methodology captures the essence of the FZ approach, while retaining the ability to treat multiple interfaces entrained within the plastic zone.
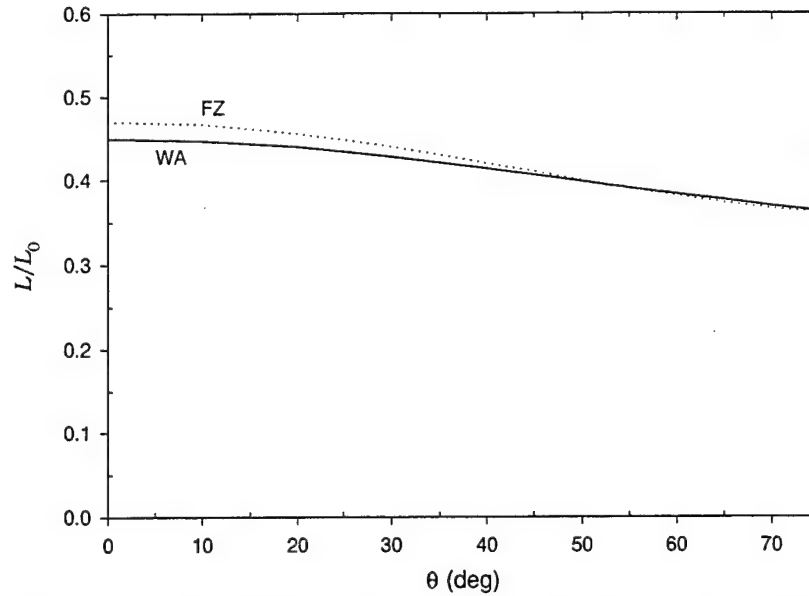
Figure 14. Comparison for FZ and revised (WA) formulations for Residual Length vs. Obliquity.
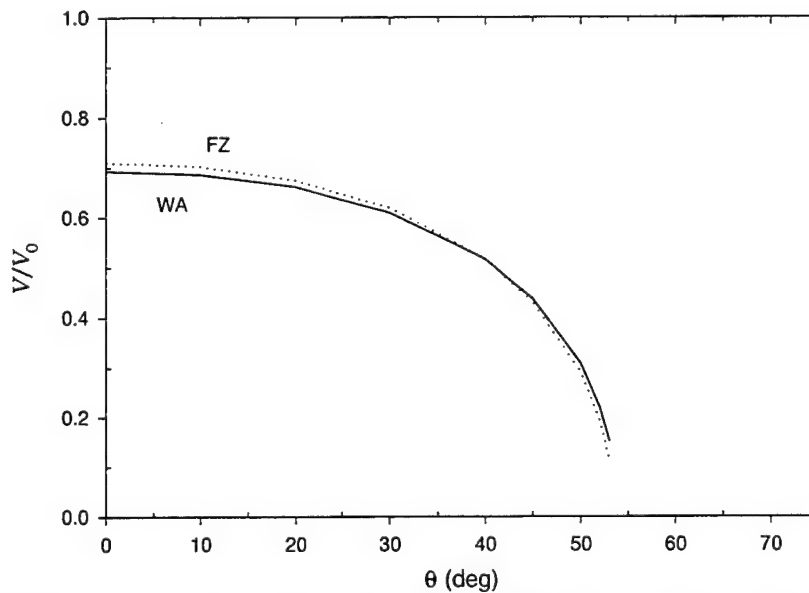
Figure 15. Comparison for FZ and revised (WA) formulations for Residual Velocity vs. Obliquity.

5.5.2 Surface Resistance. The FZ methodology contains a provision for what is called surface resistance. Though this parameter could, in theory, be used to model a target element whose strength changes over the distance from the element surface to its core, it appears that the more conventional utilization of the parameter is to characterize the phenomenon known as ceramic interface-defeat in a simple, *ad hoc* manner. The parameter, with units of resistance,

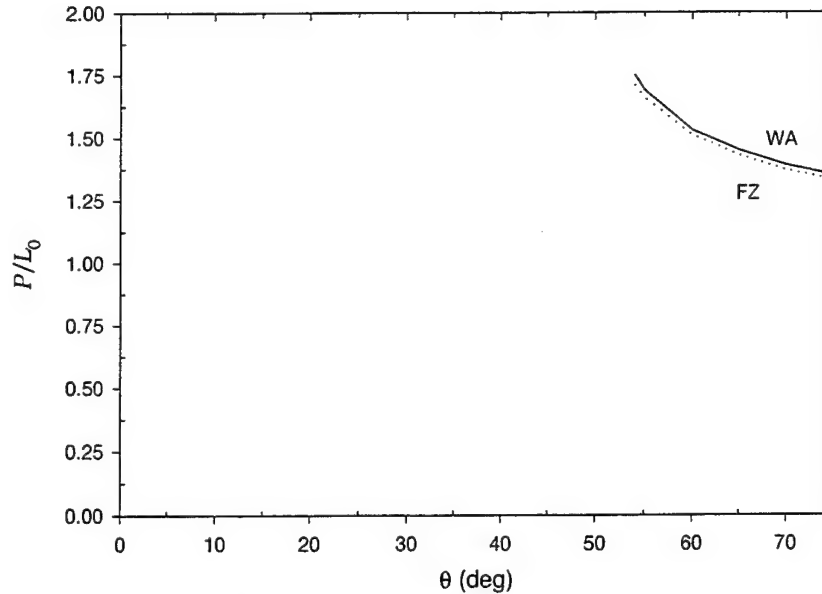**Figure 16. Comparison for FZ and revised (WA) formulations for Nonperforating Penetration vs. Obliquity.**

does not quantify a material characteristic of the ceramic, but is determined so as to best fit a known ballistic data set of interest.

Regardless of the motivation for the utilization of surface resistance in FZ methodology, the parameter is designed to behave so that the target resistance of a thick target element varies smoothly from the surface resistance to the core resistance. (In the case of partial interface-defeat, the ceramic surface resistance degrades from a high surface resistance to a lower core resistance.) The user of FZ methodology lacks control over the manner of resistance variation, only the endpoints (surface and core resistances). The FZ algorithm affects this resistance variation using the same exponential decay (or growth) form that is employed when transitioning from one target element into the next. When a thin target element possesses a surface resistance, there are two competing exponential functions determining the local effective material resistance, according to FZ methodology: one alters the target resistance from the surface resistance (forward) to the core, while, superimposed, the subsequent target element influences the target resistance (backward) prior to actually reaching that target/target interface.

The approach adopted for the revised methodology is to consider a certain thickness at the front of the target element to possess the so-called surface resistance, followed by the remainder

28

of the element (if any) at the core-resistance value. The thickness of this surface region is taken exactly as that of the constant plastic-zone thickness, ξD, associated with that target element.[*] By proceeding in this manner, the effective target resistance, as computed via equation (24), begins at the surface resistance and immediately begins growing (or decaying), finally reaching the core resistance at a distance equal to the plastic-zone thickness beneath the target surface. While this technique has the valid criticism that a change in the plastic-zone thickness has the net effect of inadvertently changing the effective surface resistance, it must be recalled that the surface resistance was not intended to characterize a material parameter in the first place, as the FZ implementation provides no latitude for specifying the manner in which the surface blends into the core. If one accepts this parameter only for its *ad hoc* utility to help characterize target elements that ballistically exhibit unique surface phenomena, then the revised implementation provides the same utility, in that regard, as the original FZ methodology.

6. Summary

With new classes of ballistic targets emerging, anticipated to comprise thin-element layers (or even continuously varying property layers), the Frank-Zook (FZ) methodology, by which terminal-ballistic penetration is currently modeled, was revisited. Though exemplary at modeling penetration through thick layered targets, with occasional material interfaces, a problem was identified with the FZ methodology when layers of target material were small compared to the penetrator diameter. Not only will this situation arise when the target-element layers are intrinsically thin or continuously varying in property, but it can also arise for the case of thicker target elements when the terminal-ballistic shotline, by design or chance, barely clips the target element. In the context of V/L codes employed in the ARL, a random shotline selection process is often employed to statistically probe the vulnerability of a target vehicle. For such situations, the V/L code user has little control over specific shotline selection, therefore making the problem of target-element clipping manifest. The penetration algorithms of these V/L codes should be made insensitive to this possibility.

---

[*] If the target-element thickness exceeds $2 \cdot \xi D$, the surface resistance will fully blend into the core resistance before the next target element exerts any influence. If the target-element thickness is between one and two times ξD, there will exist an overlap region where surface resistance and the next target element both influence the effective resistance away from the value in the core. Finally, if the target thickness is less than ξD, the target-element's core resistance will be totally subsumed by the influence of the surface resistance and the next-element influence and thereby plays no role.

With the problem thus identified, an effort was undertaken to remedy the situation, with a minimal of modification to the existing FZ methodology. To this end, elements of the Walker-Anderson (WA) model were extracted and incorporated into the FZ methodology. Key in this respect were two notions: (1) that nonsteady terms of the governing equations (whose influence increases during fluctuations associated with target-element transition) be retained and (2) that the instantaneous effective target properties be made to depend upon the flow-field and material properties ahead of the rod/target interface. Both of these revisions in solution strategy are believed to be important in achieving an accurate characterization of terminal-ballistic target classes that employ thin-element or continuously varying layers.

The implementation satisfies a primary requirement in that the modifications implemented to improve the ability of FZ methodology to address thin-element laminates has not hindered its ability to address projectile/target classes for which it had already been well suited. Those classes for which FZ was previously well suited include penetration of high- and low-L/D penetrators into either monolithic targets or targets with occasional material-interface transitions, at normal or oblique angles of incidence over a wide range of velocities of ballistic interest.

The current revisions to the FZ algorithm specifically strive to prevent an inaccurate terminal-ballistic characterization from arising for those targets possessing one or more thin target-element layers. To do this, the revised algorithm dynamically formulates the target's kinematic and material properties by way of an integration process through the plastic zone in the target, ahead of the rod/target interface. As various target layers become entrained in this plastic zone over time, their material properties begin influencing the effective (aggregate) properties of the target. Furthermore, the target forces that kinematically arise because of nonsteady penetration (*i.e.*, accelerations of the rod/target interface) are retained in this revised formulation. Such terms, previously neglected, are expected to retain a significant magnitude in those penetration events that are dominated by transient phenomena. A final extension to the FZ algorithm that was not part of WA theory is a model to compute the profile of the penetration crater. This optional algorithm is based on the notion that the rate of crater volume growth in a target may be related to both the rate at which energy is deposited by the penetrator and the

penetration resistance of the target. Though such data are not currently employed in V/L code methodology, such data might prove useful in future revisions to their methodology.

INTENTIONALLY LEFT BLANK.

7. References

1. Dibelka, R. Personal communication. Aberdeen Proving Ground, Maryland, February 2000.

2. Tate, A. "A Theory for the Deceleration of Long Rods After Impact." *Journal of Mechanics and Physics of Solids*, vol. 15, pp. 387–399, 1967.

3. Alekseevskii, V. P. "Penetration of a Rod Into a Target at High Velocity." *Combustion Explosions and Shock Waves*, vol. 2, pp. 63–66, 1966.

4. Zook, J. A., K. Frank, and G. F. Silsby. "Terminal Ballistics Test and Analysis Guidelines for the Penetration Mechanics Branch." BRL-MR-3960, U. S. Army Ballistic Research Laboratory, Aberdeen Proving Ground, Maryland, January 1992.

5. Wright, T. W., and K. Frank. "Approaches to Penetration Problems." BRL-TR-2957, U. S. Army Ballistic Research Laboratory Aberdeen Proving Ground, Maryland, December 1988.

6. Tate, A. "Long Rod Penetration Models - Part I. A Flow Field Model for High Speed Long Rod Penetration." *International Journal of Mechanical Science.*, vol. 28, no. 8, pp. 535–547, 1986.

7. Walker, J. D., and C. E. Anderson, Jr. "A Time-Dependent Model for Long-Rod Penetration." *International Journal of Impact Engineering*, vol. 16, no. 1, pp. 19–48, 1995.

8. Segletes, S. B., and W. P. Walters. "A Note on the Application of the Extended Bernoulli Equation." ARL-TR-1895, U. S. Army Research Laboratory, Aberdeen Proving Ground, Maryland, February 1999.

9. Bjerke, T. W., G. F. Silsby, D. R. Scheffler, and R. M. Mudd. "Yawed Long-Rod Armor Penetration." *International Journal of Impact Engineering*, vol. 12, no. 2, pp. 281–292, 1992.

INTENTIONALLY LEFT BLANK.

NO. OF COPIES	ORGANIZATION
2	DEFENSE TECHNICAL INFORMATION CENTER DTIC DDA 8725 JOHN J KINGMAN RD STE 0944 FT BELVOIR VA 22060-6218
1	HQDA DAMO FDT 400 ARMY PENTAGON WASHINGTON DC 20310-0460
1	OSD OUSD(A&T)/ODDDR&E(R) R J TREW THE PENTAGON WASHINGTON DC 20301-7100
1	DPTY CG FOR RDA US ARMY MATERIEL CMD AMCRDA 5001 EISENHOWER AVE ALEXANDRIA VA 22333-0001
1	INST FOR ADVNCD TCHNLGY THE UNIV OF TEXAS AT AUSTIN PO BOX 202797 AUSTIN TX 78720-2797
1	DARPA B KASPAR 3701 N FAIRFAX DR ARLINGTON VA 22203-1714
1	NAVAL SURFACE WARFARE CTR CODE B07 J PENNELLA 17320 DAHLGREN RD BLDG 1470 RM 1101 DAHLGREN VA 22448-5100
1	US MILITARY ACADEMY MATH SCI CTR OF EXCELLENCE MADN MATH MAJ HUBER THAYER HALL WEST POINT NY 10996-1786

NO. OF COPIES	ORGANIZATION
1	DIRECTOR US ARMY RESEARCH LAB AMSRL D D R SMITH 2800 POWDER MILL RD ADELPHI MD 20783-1197
1	DIRECTOR US ARMY RESEARCH LAB AMSRL DD 2800 POWDER MILL RD ADELPHI MD 20783-1197
1	DIRECTOR US ARMY RESEARCH LAB AMSRL CI AI R (RECORDS MGMT) 2800 POWDER MILL RD ADELPHI MD 20783-1145
3	DIRECTOR US ARMY RESEARCH LAB AMSRL CI LL 2800 POWDER MILL RD ADELPHI MD 20783-1145
1	DIRECTOR US ARMY RESEARCH LAB AMSRL CI AP 2800 POWDER MILL RD ADELPHI MD 20783-1197

ABERDEEN PROVING GROUND

4	DIR USARL AMSRL CI LP (BLDG 305)

35

1   US ARMY DUSA OPS RSCH
D WILLARD
102 ARMY PENTAGON
WASHINGTON DC 20310-0102

5   DEFENSE NUCLEAR AGENCY
MAJ J LYON
CDR K W HUNTER
T FREDERICKSON
R J LAWRENCE
SPSP K KIBONG
6801 TELEGRAPH RD
ALEXANDRIA VA 22310-3398

3   COMMANDER
US ARMY ARDEC
AMSTA AR FSA E
W P DUNN
J PEARSON
E BAKER
PICATINNY ARSENAL NJ 07806-5000

1   COMMANDER
US ARMY ARDEC
AMSTA AR CCH V M D NICOLICH
PICATINNY ARSENAL NJ 07806-5000

1   COMMANDER
US ARMY ARDEC
E ANDRICOPOULOS
PICATINNY ARSENAL NJ 07806-5000

1   COMMANDER
USA STRATEGIC DEFNS CMD
CSSD H LL T CROWLES
HUNTSVILLE AL 35807-3801

3   COMMANDER
US ARMY MICOM
AMSMI RD ST WF
S HILL
D LOVELACE
M SCHEXNAYDER
REDSTONE ARSENAL AL 35898-5250

1   MIS DEFNS & SPACE TECHNOLOGY
CSSD SD T K H JORDAN
PO BOX 1500
HUNTSVILLE AL 34807-3801

3   COMMANDER
US ARMY RESEARCH OFFICE
K IYER
J BAILEY
S F DAVIS
PO BOX 12211
RESEARCH TRIANGLE PARK NC 27709-2211

1   NAVAL AIR WARFARE CTR
S A FINNEGAN
BOX 1018
RIDGECREST CA 93556

4   COMMANDER
NAVAL WEAPONS CENTER
N FASIG CODE 3261
T T YEE CODE 3263
D THOMPSON CODE 3268
W J MCCARTER CODE 6214
CHINA LAKE CA 93555

12   COMMANDER
NAVAL SURFACE WARFARE CTR
DAHLGREN DIVISION
H CHEN
D L DICKINSON CODE G24
C R ELLINGTON
C R GARRETT CODE G22
W HOLT CODE G22
W E HOYE CODE G22
R MCKEOWN
J M NELSON
M J SILL CODE H11
W J STROTHER
A B WARDLAW JR
L F WILLIAMS CODE G33
17320 DAHLGREN RD
DAHLGREN VA 22448

5   AIR FORCE ARMAMENT LAB
AFATL DLJW
W COOK
M NIXON
AFATL DLJR J FOSTER
AFATL MNW
LT D LOREY
R D GUBA
EGLIN AFB FL 32542

NO. OF COPIES	ORGANIZATION	NO. OF COPIES	ORGANIZATION

<table>
<tr><td>1</td><td>USAF PHILLIPS LABORATORY
VTSI
R ROYBAL
KIRTLAND AFB NM 87117-7345</td></tr>
<tr><td>2</td><td>USAF PHILLIPS LABORATORY
PL WSCD F ALLAHDADI
PV VTA D SPENCER
3550 ABERDEEN AVE SE
KIRTLAND AFB NM 87117-5776</td></tr>
<tr><td>5</td><td>WRIGHT LABS
MNMW J W HOUSE
ARMAMENT DIRECTORATE STE 326 B1
R D HUNT
B MILLIGAN
B C PATTERSON
W H VAUGHT
101 W EGLIN BLVD
EGLIN AFB FL 32542-6810</td></tr>
<tr><td>1</td><td>AFIT ENC
D A FULK
WRIGHT PATTERSON AFB OH 45433</td></tr>
<tr><td>9</td><td>LOS ALAMOS NATIONAL LABORATORY
L HULL MS A133
J V REPA MS A133
J WALTERMS C305
C WINGATE MS D413
W SPARKS MS F663
E J CHAPYAK MS F664
J BOLSTAD MS G787
P HOWE MS P915
J KENNEDY MS P915
PO BOX 1663
LOS ALAMOS NM 87545</td></tr>
<tr><td>8</td><td>SANDIA NATIONAL LABORATORIES
MAIL SERVICES MS-0100
E W REECE   MS 0307
D P KELLY   MS 0307
L WEIRICK   MS 0327
R TACHAU   MS 0425
D LONGCOPE MS 0439
D HAYES   MS 0457
J ASAY   MS 0458
W TEDESCHI MS 0482
PO BOX 5800
ALBUQUERQUE NM 87185-0100</td></tr>
</table>

Second column:

NO. OF COPIES	ORGANIZATION
29	SANDIA NATIONAL LABORATORIES MAIL SERVICES MS-0100 J SCHULZE MS 0483 P A LONGMIRE MS 0560 J COREY MS 0576 E S HERTEL JR MS 0819 A ROBINSON MS 0819 T TRUCANO MS 0819 J M MCGLAUN MS 0819 M VIGIL MS 0819 R BRANNON MS 0820 J ANG MS 0821 M BOSLOUGH MS 0821 D CRAWFORD MS 0821 M FURNISH MS 0821 C HALL MS 0821 W REINHART MS 0821 P STANTON MS 0821 M KIPP DIV 1533 P YARRINGTON DIV 1533 J MCGLAWA DIV 1541 M FORRESTAL DIV 1551 R LAFARGE DIV 1551 C HILLS DIV 1822 P TAYLOR ORG 1432 B LEVIN ORG 7816 L N KMETYK R REEDER J SOUTHWARD C KONRAD K LANG PO BOX 5800 ALBUQUERQUE NM 87185-0100
4	DIRECTOR LLNL MS L35 R E TIPTON D BAUM T MCABEE M MURPHY PO BOX 808 LIVERMORE CA 94550

NO. OF COPIES	ORGANIZATION	NO. OF COPIES	ORGANIZATION
7	DIRECTOR LLNL MS L122 R PIERCE R ROSINKY O J ALFORD D STEWART T VIDLAK B R BOWMAN W DIXON PO BOX 808 LIVERMORE CA 94550	2	DIRECTOR LLNL MS L290 A HOLT J E REAUGH PO BOX 808 LIVERMORE CA 94550
2	DIRECTOR LLNL MS L125 D R FAUX N W KLINO PO BOX 808 LIVERMORE CA 94550	4	ENERGETIC MATLS RSCH TSTNG CTR NEW MEXICO TECH D J CHAVEZ M LEONE L LIBERSKY F SANDSTROM CAMPUS STATION SOCORRO NM 87801
1	DIRECTOR LLNL R BARKER L159 PO BOX 808 LIVERMORE CA 94550	3	NASA JOHNSON SPACE CENTER E CHRISTIANSEN J L CREWS F HORZ MAIL CODE SN3 2101 NASA RD 1 HOUSTON TX 77058
2	DIRECTOR LLNL MS L180 G SIMONSON A SPERO PO BOX 808 LIVERMORE CA 94550	1	APPLIED RESEARCH LAB J A COOK 10000 BURNETT ROAD AUSTIN TX 78758
1	DIRECTOR LLNL F A HANDLER L182 PO BOX 808 LIVERMORE CA 94550	5	JET PROPULSION LABORATORY IMPACT PHYSICS GROUP Z SEKANINA P WEISSMAN B WEST J ZWISSLER M ADAMS 4800 OAK GROVE DR PASADENA CA 91109
1	DIRECTOR LLNL MS L282 W TAO PO BOX 808 LIVERMORE CA 94550	1	DREXEL UNIVERSITY MEM DEPT 32ND & CHESTNUT ST PHILADELPHIA PA 19104

39

1 G E DUVALL
 5814 NE 82ND COURT
 VANCOUVER WA 98662-5944

3 DYNA EAST CORP
 P C CHOU
 R CICCARELLI
 W FLIS
 3620 HORIZON DRIVE
 KING OF PRUSSIA PA 19406

3 DYNASEN
 J CHAREST
 M CHAREST
 M LILLY
 20 ARNOLD PL
 GOLETA CA 93117

1 R J EICHELBERGER
 409 W CATHERINE ST
 BEL AIR MD 21014-3613

1 ELORET INSTITUTE
 D W BOGDANOFF MS 230 2
 NASA AMES RESEARCH CENTER
 MOFFETT FIELD CA 94035

1 RAYTHEON MSL SYS CO
 T STURGEON
 BLDG 805 M/S D4
 PO BOX 11337
 TUCSON AZ 85734-1337

5 INST OF ADVANCED TECHNOLOGY
 UNIVERSITY OF TX AUSTIN
 S J BLESS
 J CAZAMIAS
 J DAVIS
 H D FAIR
 D LITTLEFIELD
 4030-2 W BRAKER LN
 AUSTIN TX 78759

1 INTERNATIONAL RESEARCH ASSOC
 D L ORPHAL
 4450 BLACK AVE
 PLEASANTON CA 94566

1 INTERPLAY
 F E WALKER
 18 SHADOW OAK RD
 DANVILLE CA 94526

1 ITT SCIENCES AND SYSTEMS
 J WILBECK
 600 BLVD SOUTH
 SUITE 208
 HUNTSVILLE AL 35802

1 R JAMESON
 624 ROWE DR
 ABERDEEN MD 21001

1 KAMAN SCIENCES CORP
 D L JONES
 2560 HUNTINGTON AVE SUITE 200
 ALEXANDRIA VA 22303

7 KAMAN SCIENCES CORP
 J ELDER
 R P HENDERSON
 D A PYLES
 F R SAVAGE
 J A SUMMERS
 T W MOORE
 T YEM
 600 BLVD S SUITE 208
 HUNTSVILLE AL 35802

3 KAMAN SCIENCES CORP
 S JONES
 G L PADEREWSKI
 R G PONZINI
 1500 GRDN OF THE GODS RD
 COLORADO SPRINGS CO 80907

4 KAMAN SCIENCES CORP
 N ARI
 S R DIEHL
 W DOANE
 V M SMITH
 PO BOX 7463
 COLORADO SPRINGS CO 80933-7463

1 D R KENNEDY & ASSOC INC
 D KENNEDY
 PO BOX 4003
 MOUNTAIN VIEW CA 94040

1	KERLEY PUBLISHING SERVICES G I KERLEY PO BOX 13835 ALBUQUERQUE NM 87192-3835
1	LOCKHEED MARTIN ELEC & MSLS G W BROOKS 5600 SAND LAKE RD MP 544 ORLANDO FL 32819-8907
1	LOCKHEED MARTIN MISSLE & SPACE W R EBERLE PO BOX 070017 HUNTSVILLE AL 35807
1	MCDONNELL DOUGLAS ASTRONAUTICS CO B L COOPER 5301 BOLSA AVE HUNTINGTON BEACH CA 92647
1	NETWORK COMPUTING SERVICES INC T HOLMQUIST 1200 WASHINGTON AVE S MINNEAPOLIS MN 55415
4	ORLANDO TECHNOLOGY INC D A MATUSKA M GUNGER J OSBORN R SZEZEPANSKI PO BOX 855 SHALIMAR FL 32579-0855
1	PHYSICAL SCIENCES INC P NEBOLSINE 20 NEW ENGLAND BUS CTR ANDOVER MA 01810
5	PRIMEX TECHNOLOGIES INC G FRAZIER L GARNETT D OLIVER D TUERPE J COFFENBERRY 2700 MERCED ST SAN LEANDRO CA 94577-0599

1	RAYTHEON ELECTRONIC SYSTEMS R LLOYD 50 APPLE HILL DRIVE TEWKSBURY MA 01876
2	TELEDYNE BROWN ENGR J W BOOTH M B RICHARDSON PO BOX 070007 MS 50 HUNTSVILLE AL 35807-7007
1	ZERNOW TECHNICAL SVCS INC L ZERNOW 425 W BONITA AVE SUITE 208 SAN DIMAS CA 91773

ABERDEEN PROVING GROUND

22	DIR, USARL
	AMSRL-SL-BD
	   D BELY
	   R GROTE
	   J POLESNE
	   R SAUCIER
	AMSRL-SL-EA, J A MORRISSEY
	AMSRL-WM-BC, A ZIELINSKI
	AMSRL-WM-BE, S L HOWARD
	AMSRL-WM-MB, G GAZONAS
	AMSRL-WM-T, T W WRIGHT
	AMSRL-WM-TA,
	   W GILLICH
	   M BURKINS
	   W BRUCHEY
	   J DEHN
	   W A GOOCH
	   E HORWATH
	   H W MEYER
	   M NORMANDIA
	   J RUNYEON
	AMSRL-WM-TB,
	   R FREY
	   P BAKER
	   R LOTTERO
	   J STARKENBERG

NO. OF
COPIES   ORGANIZATION

23   DIR, USARL
        AMSRL-WM-TC,
            R COATES
            T W BJERKE
            K KIMSEY
            M LAMPSON
            L MAGNESS
            D SCHEFFLER
            S SCHRAML
            G SILSBY
            B SORENSEN
            R SUMMERS
            W WALTERS
        AMSRL-WM-TD,
            A M DIETRICH
            D DANDEKAR
            T FARRAND
            K FRANK
            M RAFTENBERG
            G RANDERS-PEHRSON, LLNL
            E J RAPACKI
            M SCHEIDLER
            S SCHOENFELD
            S SEGLETES (2 CPS)
            T WEERISOORIYA

NO. OF COPIES	ORGANIZATION
3	AERONAUTICAL & MARITIME RESEARCH LABORATORY N BURMAN S CIMPOERU D PAUL PO BOX 4331 MELBOURNE VIC 3001 AUSTRALIA
1	PRB S A M VANSNICK AVENUE DE TERVUEREN 168 BTE 7 BRUSSELS B 1150 BELGIUM
2	ROYAL MILITARY ACADEMY G DYCKMANS E CELENS RENAISSANCE AVE 30 B1040 BRUSSELS BELGIUM
1	CANADIAN ARSENALS LTD P PELLETIER 5 MONTEE DES ARSENAUX VILLIE DE GRADEUR PQ J5Z2 CANADA
1	DEFENCE RSCH ESTAB SUFFIELD D MACKAY RALSTON ALBERTA TOJ 2NO RALSTON CANADA
1	DEFENCE RSCH ESTAB SUFFIELD C WEICKERT BOX 4000 MEDICINE HAT ALBERTA TIA 8K6 CANADA
1	DEFENCE RSCH ESTAB VALCARTIER ARMAMENTS DIVISION R DELAGRAVE 2459 PIE X1 BLVD N PO BOX 8800 CORCELETTE QUEBEC GOA 1R0 CANADA

NO. OF COPIES	ORGANIZATION
1	CEA R CHERET CEDEX 15 313 33 RUE DE LA FEDERATION PARIS 75752 FRANCE
1	CEA CISI BRANCH P DAVID CENTRE DE SACLAY BP 28 GIF SUR YVETTE 91192 FRANCE
1	CEA/CESTA A GEILLE BOX 2 LE BARP 33114 FRANCE
5	CENTRE D'ETUDES DE GRAMAT C LOUPIAS P OUTREBON J CAGNOUX C GALLIC J TRANCHET GRAMAT 46500 FRANCE
3	CENTRE D'ETUDES DE VAUJOURS J-P PLOTARD E BOTTET TAT SIHN VONG BOITE POSTALE NO 7 COUNTRY 77181 FRANCE
6	CENTRE DE RECHERCHES ET D'ETUDES D'ARCUEIL D BOUVART C COTTENNOT S JONNEAUX H ORSINI S SERROR F TARDIVAL 16 BIS AVENUE PRIEUR DE LA COTE D'OR F94114 ARCUEIL CÉDEX FRANCE

NO. OF COPIES	ORGANIZATION	NO. OF COPIES	ORGANIZATION
1	DAT ETBS CETAM C ALTMAYER ROUTE DE GUERRY BOURGES 18015 FRANCE	1	DIEHL GBMH AND CO M SCHILDKNECHT FISCHBACHSTRASSE 16 D 90552 RÖTBENBACH AD PEGNITZ GERMANY
1	ETBS DSTI P BARNIER ROUTE DE GUERAY BOITE POSTALE 712 18015 BOURGES CEDEX FRANCE	3	FRAUNHOFER INSTITUT FUER KURZZEITDYNAMIK ERNST MACH INSTITUT H ROTHENHAEUSLER H SENF E STRASSBURGER KLINGELBERG 1 D79588 EFRINGEN-KIRCHEN GERMANY
1	FRENCH GERMAN RESEARCH INST P-Y CHANTERET CEDEX 12 RUE DE I'INDUSTRIE BP 301 F68301 SAINT-LOUIS FRANCE	3	FRENCH GERMAN RESEARCH INST G WEIHRAUCH R HUNKLER E WOLLMANN POSTFACH 1260 WEIL AM RHEIN D-79574 GERMANY
5	FRENCH GERMAN RESEARCH INST H-J ERNST F JAMET P LEHMANN K HOOG H F LEHR CEDEX 5 5 RUE DU GENERAL CASSAGNOU SAINT LOUIS 68301 FRANCE	2	IABG M BORRMANN H G DORSCH EINSTEINSTRASSE 20 D 8012 OTTOBRUN B MUENCHEN GERMANY
1	BATTELLE INGENIEUTECHNIK GMBH W FUCHE DUESSELDORFFER STR 9 ESCHBORN D 65760 GERMANY	1	INGENIEURBÜRO DEISENROTH AUF DE HARDT 33 35 D5204 LOHMAR 1 GERMANY
1	CONDAT J KIERMEIR MAXIMILIANSTR 28 8069 SCHEYERN FERNHAG GERMANY	5	RAFAEL BALLISTICS CENTER E DEKEL Y PARTOM G ROSENBERG Z ROSENBERG Y YESHURUN PO BOX 2250 HAIFA 31021 ISRAEL
1	DEUTSCHE AEROSPACE AG M HELD POSTFACH 13 40 D 86523 SCHROBENHAUSEN GERMANY		

1   TECHNION INST OF TECH
FACULTY OF MECH ENGNG
S BODNER
TECHNION CITY
HAIFA 32000
ISRAEL

1   IHI RESEARCH INSTITUTE
STRUCTURE & STRENGTH
T SHIBUE
1-15, TOYOSU 3
KOTO, TOKYO 135
JAPAN

1   ESTEC CS
D CASWELL
BOX 200 NOORDWIJK
2200 AG
NETHERLANDS

4   PRINS MAURITS LABORATORY
H J REITSMA
E VAN RIET
H PASMAN
R YSSELSTEIN
TNO BOX 45
RIJSWIJK 2280AA
NETHERLANDS

1   ROYAL NETHERLANDS ARMY
J HOENEVELD
V D BURCHLAAN 31
PO BOX 90822
2509 LS THE HAGUE
NETHERLANDS

3   INSTITUTE OF MECH ENGNG PROBLEMS
V BULATOV
D INDEITSEV
Y MESCHERYAKOV
BOLSHOY, 61, V.O.
ST PETERSBURG 199178
RUSSIAN REPUBLIC

1   IPE RAS
A A BOGOMAZ
DVORTSOVAIA NAB 18
ST PETERSBURG
RUSSIAN REPUBLIC

2   LAVRENTYEV INST. HYDRODYNAMICS
L A MERZHIEVSKY
VICTOR V SILVESTROV
630090 NOVOSIBIRSK
RUSSIAN REPUBLIC

1   MOSCOW INST OF PHYSICS & TECH
S V UTYUZHNIKOV
DEPT OF COMPUTATIONAL
MATHEMATICS
DOLGOPRUDNY 1471700
RUSSIAN REPUBLIC

1   RESEARCH INSTITUTE OF MECHANICS
NIZHNIY NOVGOROD STATE UNIVERSITY
A SADYRIN
P.R. GAYARINA 23 KORP 6
NIZHNIY NOVGOROD 603600
RUSSIAN REPUBLIC

1   SAMARA STATE AEROSPACE UNIV
L G LUKASHEV
SAMARA
RUSSIAN REPUBLIC

1   TOMSK BRANCH OF THE INSTITUTE
FOR STRUCTURAL MACROKINETICS
V GORELSKI
8 LENIN SQ GSP 18
TOMSK 634050
RUSSIAN REPUBLIC

1   DYNAMEC RESEARCH AB
Å PERSSON
P.O. BOX 201
S-151 23 SÖDERTÄLJE
SWEDEN

6   NATL DEFENCE RESEARCH EST
L HOLMBERG
U LINDEBERG
L G OLSSON
L HOLMBERG
B JANZON
I MELLGARD
FOA BOX 551
TUMBA S-14725
SWEDEN

2	SWEDISH DEFENCE RSCH ESTAB DIVISION OF MATERIALS S J SAVAGE J ERIKSON STOCKHOLM S-17290 SWEDEN
2	K&W THUN W LANZ W ODERMATT ALLMENDSSTRASSE 86 CH-3602 THUN SWITZERLAND
2	AWE M GERMAN W HARRISON FOULNESS ESSEX SS3 9XE UNITED KINGDOM
2	DERA I CULLIS J P CURTIS FORT HALSTEAD SEVENOAKS KENT TN14 7BP UNITED KINGDOM
6	DEFENCE RESEARCH AGENCY W A J CARSON I CROUCH C FREW T HAWKINS B JAMES B SHRUBSALL CHOBHAM LANE CHERTSEY SURREY KT16 0EE UNITED KINGDOM
1	UK MINISTRY OF DEFENCE G J CAMBRAY CBDE PORTON DOWN SALISBURY WITTSHIRE SPR 0JQ UNITED KINGDOM

7	INSTITUTE FOR PROBLEMS IN MATERIALS STRENGTH S FIRSTOV B GALANOV O GRIGORIEV V KARTUZOV V KOVTUN Y MILMAN V TREFILOV 3, KRHYZHANOVSKY STR 252142, KIEV-142 UKRAINE
1	INSTITUTE FOR PROBLEMS OF STRENGTH G STEPANOV TIMIRYAZEVSKAYU STR 2 252014 KIEV UKRAINE

REPORT DOCUMENTATION PAGE

1. AGENCY USE ONLY *(Leave blank)*	2. REPORT DATE	3. REPORT TYPE AND DATES COVERED
	September 2000	Final, Oct 98 - Jul 00

4. TITLE AND SUBTITLE

An Adaptation of Walker-Anderson Model Elements Into the Frank-Zook Penetration Model for Use in MUVES

5. FUNDING NUMBERS

AH80

6. AUTHOR(S)

Steven B. Segletes

7. PERFORMING ORGANIZATION NAME(S) AND ADDRESS(ES)

U.S. Army Research Laboratory
ATTN: AMSRL-WM-TD
Aberdeen Proving Ground, MD 21010-5066

8. PERFORMING ORGANIZATION REPORT NUMBER

ARL-TR-2336

9. SPONSORING/MONITORING AGENCY NAMES(S) AND ADDRESS(ES)

10. SPONSORING/MONITORING AGENCY REPORT NUMBER

11. SUPPLEMENTARY NOTES

12a. DISTRIBUTION/AVAILABILITY STATEMENT

Approved for public release; distribution is unlimited.

12b. DISTRIBUTION CODE

13. ABSTRACT*(Maximum 200 words)*

The performance of the well-respected Frank-Zook (FZ) penetration algorithm is examined in light of an anticipated class of target technology involving laminated targets whose layers are thin relative to the projectile diameter (in the limiting case, this target class incorporates functionally graded materials). Because of the manner in which the FZ algorithm anticipates changes in material properties along the shotline of the penetrator, the algorithm is susceptible to inaccuracy precisely when the target layers along the shotline are thin relative to the projectile diameter. Though the problem can be quite severe when the target-layer thickness is a fraction of the projectile diameter, the effect is still evident to a much lesser extent, even as the target-element thickness is increased to several projectile diameters. A remedy to this type of problem is offered, accomplished by way of novel adaptation of elements of a model by Walker and Anderson into the FZ framework. In doing so, the target's material- and nonsteady-kinematic properties are dynamically composed via an integration through the plastic zone in the target, ahead of the rod/target interface. Additionally, a model to predict the crater-diameter profile resulting from a modeled penetration event is optionally offered as a calculation enhancement. The modeling remedies and enhancements proposed herein are offered for incorporation into the U.S. Army Research Laboratory's (ARL) modular Unix-based vulnerability estimation suite (MUVES) code, to be part of ARL's vulnerability/lethality (V/L) calculation methodology.

14. SUBJECT TERMS			15. NUMBER OF PAGES
penetration mechanics, plasticity, target resistance, effective density			49
			16. PRICE CODE

17. SECURITY CLASSIFICATION OF REPORT	18. SECURITY CLASSIFICATION OF THIS PAGE	19. SECURITY CLASSIFICATION OF ABSTRACT	20. LIMITATION OF ABSTRACT
UNCLASSIFIED	UNCLASSIFIED	UNCLASSIFIED	UL

INTENTIONALLY LEFT BLANK.

USER EVALUATION SHEET/CHANGE OF ADDRESS

This Laboratory undertakes a continuing effort to improve the quality of the reports it publishes. Your comments/answers to the items/questions below will aid us in our efforts.

1. ARL Report Number/Author ARL-TR-2336 (Segletes) _____ Date of Report September 2000 _____

2. Date Report Received _____

3. Does this report satisfy a need? (Comment on purpose, related project, or other area of interest for which the report will be used.) _____

_____

_____

4. Specifically, how is the report being used? (Information source, design data, procedure, source of ideas, etc.) _____

_____

_____

5. Has the information in this report led to any quantitative savings as far as man-hours or dollars saved, operating costs avoided, or efficiencies achieved, etc? If so, please elaborate. _____

6. General Comments. What do you think should be changed to improve future reports? (Indicate changes to organization, technical content, format, etc.) _____

_____

_____

_____

Organization _____

CURRENT   Name _____   E-mail Name _____
ADDRESS
               Street or P.O. Box No. _____

               City, State, Zip Code _____

7. If indicating a Change of Address or Address Correction, please provide the Current or Correct address above and the Old or Incorrect address below.

Organization _____

OLD   Name _____
ADDRESS
               Street or P.O. Box No. _____

               City, State, Zip Code _____

(Remove this sheet, fold as indicated, tape closed, and mail.)
(DO NOT STAPLE)

DEPARTMENT OF THE ARMY

OFFICIAL BUSINESS

BUSINESS REPLY MAIL
FIRST CLASS PERMIT NO 0001,APG,MD

POSTAGE WILL BE PAID BY ADDRESSEE

DIRECTOR
US ARMY RESEARCH LABORATORY
ATTN AMSRL WM TD
ABERDEEN PROVING GROUND MD 21005-5066

NO POSTAGE
NECESSARY
IF MAILED
IN THE
UNITED STATES